

# Surrogate-based optimization using an artificial neural network for a parameter identification in a 3D marine ecosystem model

Markus Pfeil<sup>1</sup> and Thomas Slawig<sup>1</sup>

<sup>1</sup>Kiel Marine Science (KMS) - Centre for Interdisciplinary Marine Science, Dep. of Computer Science, Kiel University, 24098 Kiel, Germany ({mpf, ts}@informatik.uni-kiel.de).

## Abstract

Parameter identification for marine ecosystem models is important for the assessment and validation of marine ecosystem models against observational data. The surrogate-based optimization (SBO) is a computationally efficient method to optimize complex models. SBO replaces the computationally expensive (high-fidelity) model by a surrogate constructed from a less accurate but computationally cheaper (low-fidelity) model in combination with an appropriate correction approach, which improves the accuracy of the low-fidelity model. To construct a computationally cheap low-fidelity model, we tested three different approaches to compute an approximation of the annual periodic solution (i.e., a steady annual cycle) of a marine ecosystem model: firstly, a reduced number of spin-up iterations (several decades instead of millennia), secondly, an artificial neural network (ANN) approximating the steady annual cycle and, finally, a combination of both approaches. Except for the low-fidelity model using only the ANN, the SBO yielded a solution close to the target and reduced the computational effort significantly. If an ANN approximating appropriately a marine ecosystem model is available, the SBO using this ANN as low-fidelity model presents a promising and computational efficient method for the validation.

## 1 Introduction

In the field of climate research, marine ecosystem models are part and parcel of the analysis of changes in the marine ecosystem influenced by diverse biogeochemical processes. As part of the global carbon cycle, the ocean takes up, for example, CO<sub>2</sub> from the atmosphere and stores it. A marine ecosystem model consists of a global circulation model coupled with a biogeochemical model considering the interactions of the physical and biogeochemical processes (cf. Fasham 2003; Sarmiento and Gruber 2006; W. Fennel and Neumann 2004). In particular, the equations and variables describing the physical

processes are well known. Conversely, there is generally no set of equations and variables to describe the biogeochemical processes which is why many biogeochemical models exist that differ in their complexity by the number of state variables and parametrizations (see e.g., Kriest, Khatiwala, and Oschlies 2010). Therefore, validation and assessment of the biogeochemical models, which include a parameter optimization and a discussion of simulation results, are necessary by an evaluation of the model outputs against observational data (K. Fennel et al. 2001).

Parameter identification to validate biogeochemical models, especially for three-dimensional models, is a challenging task with a large computational effort. The parameter identification determines or adjusts the model parameters to fit the model to existing measurement data or a corresponding model output (Banks and Kunisch 1989). For marine ecosystem models, this corresponds to the solving of a nonlinear optimization problem that typically requires many evaluations of the model-data misfit function, also called cost or objective function. As a consequence, such optimizations using conventional optimization algorithms are very time-consuming or infeasible even on high-performance computers because a single model evaluation already is computationally expensive (Oschlies 2006). To date, the search for a feasible optimization for global marine ecosystem models has included, for instance, approaches of a statistical emulator technique as well as a gradient-free method (Kwon and Primeau 2006; Kwon and Primeau 2008; Mattern, K. Fennel, and Dowd 2012). Due to the high computational effort, the acceleration of the optimization process itself or of the underlying simulation is still of great interest.

*Surrogate-based optimization* (SBO) is a computationally efficient method to optimize complex models (so-called *high-fidelity models*), whose simple model evaluation already requires enormous computational effort (Queipo et al. 2005; Forrester and Keane 2009; Bandler et al. 2004; Leifsson and Koziel 2010). The surrogate, which is computationally cheap and a reasonable approximation of the high-fidelity model, replaces the high-fidelity model in the optimization process. Consequently, the SBO estimates the optimal parameters of the high-fidelity model by optimizing the surrogate. There are several variants to construct the surrogate, such as function-approximation surrogates (Queipo et al. 2005; Simpson et al. 2001; Smola and Schölkopf 2004) or physics-based ones (Søndergaard 2003) using a *low-fidelity model* that is a less accurate approximation of the high-fidelity model. The latter approach is used in this paper because coarser discretizations (in time and/or space) are common in climate research (McGuffie and Henderson-Sellers 2014). The application of SBO for the parameter identification of marine ecosystem models has already reduced computational costs compared to conventional optimizations because the number of high-fidelity model evaluations were much smaller (Prieß, Piwonski, et al. 2013; Prieß, Koziel, and Slawig 2011; Prieß, Koziel, and Slawig 2013).

Several strategies enable the reduction of the computational effort simulating marine ecosystem models. The fully coupled simulation of a marine ecosystem model to compute a steady annual cycle is computationally expensive because it requires a long-time integration over several millennia, but a single evaluation is already computationally expensive (cf. Bernsen, Dijkstra, and Wubs 2008; Bryan 1984; Danabasoglu, McWilliams, and Large 1996; Wunsch and Heimbach 2008; Siberlin and Wunsch 2011; Oschlies 2006).

As opposed to the fully coupled simulation (the so-called *online* simulation), the *offline* simulation neglects the impact of the biogeochemical model on the ocean circulation to reduce the computational effort using pre-computed data of the ocean currents. Moreover, the *transport matrix method* (TMM) reduces the computation of the global ocean circulation to a matrix-vector multiplication and, thus, decouples the evaluation of the biogeochemical model from the ocean circulation (Khatiwala, Visbeck, and Cane 2005; Khatiwala 2007). This approach also lowers the computational effort with a tolerable loss of accuracy. These two strategies are only two examples to reduce the computational effort.

Deep Learning enables predictions of steady annual cycles for a marine ecosystem model using the features learned from other steady annual cycles. In recent years, Deep Learning (Goodfellow, Bengio, and Courville 2016; LeCun, Bengio, and G. Hinton 2015) based on *artificial neural networks* (ANNs) allowed breakthroughs in many areas, such as classification, speech recognition, computer vision or bioinformatics. The power of Deep Learning lies in recognizing patterns in data provided to train the neural network and predicting corresponding data based on the learned patterns. We applied Deep Learning to predict steady annual cycles from model parameters so that the long-time integration was not longer necessary (Pfeil and Slawig 2021a).

The combination of a low-fidelity model and correction technique affects both the accuracy and the computational effort of the surrogate that was used for the SBO (cf. Søndergaard 2003; Prieß, Piwonski, et al. 2013). The low-fidelity model is always a compromise between the accuracy and the computational effort of the high-fidelity model approximation. An ANN offers new opportunities to approximate a steady annual cycle for the use as low-fidelity model. While the accuracy using only the ANN as low-fidelity model was not sufficient for the SBO, the SBO which used a physics-based low-fidelity model improved by the ANN showed good results. In the present paper, we applied synthetic data generated by the high-fidelity model to assess the feasibility of the SBO with the different low-fidelity models. Instead of real measurement data, the use of synthetic data avoided uncertainties, such as the required structural complexity of the model to reconstruct real measurement data, errors in the measurements and the performance of the optimization itself.

This paper is structured as follows: after an introduction into marine ecosystem models including the computation of steady annual cycles using the TMM in Section 2, Section 3 contains the description of the methods used to train an ANN together with the resulting ANN. In Section 4, we describe the SBO. Numerical results of the SBO using different low-fidelity models are presented in Section 5. The paper closes with a summary and conclusions.

## **2 Model description**

A marine ecosystem model describes the interplay between the ocean circulation and the interactions and biogeochemistry among ocean biota. The marine ecosystem is represented by a given number of ecosystem species (or tracers) which are substances in the

ocean water and subject to chemical or biochemical reactions. In the marine ecosystem model, both the ocean circulation affects the tracer concentrations and, vice versa, the tracers affect the ocean circulation. A fully coupled model (*online* model) includes both of these interactions and, hence, simulating such a model is computationally expensive and often limited to single model evaluations (Oschlies 2006). In contrast, an *offline* model simplifies the complexity by neglecting the influence of the tracers on the ocean circulation. As a result of this one-way coupling, we can use a pre-computed ocean circulation for the simulation.

## 2.1 Model equations for marine ecosystems

A system of partial differential equations models the marine ecosystem. The complexity of the marine ecosystem models varies, inter alia, by the number of tracers, which defines the size of the system of differential equations. The differential equations in the system are of the Lotka-Volterra or predator-prey type (Lotka 1910; Volterra 1931). In the rest of this paper, we consider marine ecosystem models using an offline model and  $n_y \in \mathbb{N}$  tracers on a spatial domain  $\Omega \subset \mathbb{R}^3$  (i.e., the ocean) and a time interval  $[0, 1]$  (i.e., one model year). The mapping  $y_i : \Omega \times [0, 1] \rightarrow \mathbb{R}$ ,  $i \in \{1, \dots, n_y\}$ , describes the tracer concentration of the single tracer  $y_i$  and  $\mathbf{y} := (y_i)_{i=1}^{n_y}$  summarizes the tracer concentrations of all tracers. The system of parabolic partial differential equations

$$\frac{\partial y_i}{\partial t}(x, t) + (D(x, t) + A(x, t)) y_i(x, t) = q_i(x, t, \mathbf{y}, \mathbf{u}), \quad x \in \Omega, t \in [0, 1], \quad (1)$$

$$\frac{\partial y_i}{\partial n}(x, t) = 0, \quad x \in \partial\Omega, t \in [0, 1], \quad (2)$$

for  $i = 1, \dots, n_y$ , defines the tracer transport of a marine ecosystem model. The linear operators  $A : \Omega \times [0, 1] \rightarrow \mathbb{R}$  and  $D : \Omega \times [0, 1] \rightarrow \mathbb{R}$  correspond to the advection and diffusion coming from the ocean circulation while the term  $q_i : \Omega \times [0, 1] \rightarrow \mathbb{R}$  summarizes all biogeochemical terms for the tracer  $y_i$ . The homogeneous Neumann boundary condition (2) includes the normal derivative describing an absence of fluxes on the boundary.

The spatial tracer transport in marine water depends on the ocean currents in form of spatially discretized advection and diffusion. The advection including a given velocity field  $v : \Omega \times [0, 1] \rightarrow \mathbb{R}^3$  is modeled as

$$A(x, t)y_i(x, t) := \operatorname{div}(v(x, t)y_i(x, t)), \quad x \in \Omega, t \in [0, 1] \quad (3)$$

for  $i \in \{1, \dots, n_y\}$ . The diffusion models the turbulent effects of the ocean circulation. The molecular diffusion of the tracers themselves, conversely, is neglected because this diffusion is much smaller than the diffusion induced by turbulence. In ocean circulation modeling, the quite different scales in horizontal and vertical direction requires a splitting  $D = D_h + D_v$  and an implicit treatment of the vertical part in the time integration. Both

directions of the diffusion are modeled in the second-order form as

$$D_h(x, t)y_i(x, t) := -\operatorname{div}_h(\kappa_h(x, t)\nabla_h y_i(x, t)) \quad x \in \Omega, t \in [0, 1], \quad (4)$$

$$D_v(x, t)y_i(x, t) := -\frac{\partial}{\partial z} \left( \kappa_v(x, t) \frac{\partial y_i}{\partial z}(x, t) \right), \quad x \in \Omega, t \in [0, 1] \quad (5)$$

for  $i \in \{1, \dots, n_y\}$ , where  $\operatorname{div}_h$  and  $\nabla_h$  denote the horizontal divergence and gradient,  $\kappa_h, \kappa_v : \Omega \times [0, 1] \rightarrow \mathbb{R}$  the diffusion coefficient fields and  $z$  is the vertical coordinate. Due to the neglect of the molecular diffusion, the diffusion coefficients are identical for all tracers.

The biogeochemical model summarizes the biogeochemical processes modeled in the marine ecosystem. The nonlinear function  $q_i : \Omega \times [0, 1] \rightarrow \mathbb{R}$ ,  $(x, t) \mapsto q_i(x, t, \mathbf{y}, \mathbf{u})$  describes the biogeochemical processes for the tracer  $y_i$ ,  $i \in \{1, \dots, n_y\}$ . More specifically, the biogeochemical processes depend, firstly, on the variability of the solar radiation in space and time, secondly, on the coupling to other tracers and, thirdly, on  $n_u \in \mathbb{N}$  model parameters  $\mathbf{u} \in \mathbb{R}^{n_u}$  (such as growth, loss and mortality rates or sinking speed). The biogeochemical model  $\mathbf{q} = (q_i)_{i=1}^{n_y}$  combines the biogeochemical processes for all tracers. In contrast to the biogeochemical model, the marine ecosystem model, moreover, includes the effects of the ocean circulation and, thus, comprises the whole system (1) to (6).

For the marine ecosystem model, an annual periodic solution of (1) and (2) (i.e., a steady annual cycle) fulfills

$$y_i(x, 0) = y_i(x, 1), \quad x \in \Omega, \quad (6)$$

for  $i \in \{1, \dots, n_y\}$ . For this purpose, we assume that the operators  $D, A$  and the functions  $q_i$  also are annually periodic in time.

## 2.2 Biogeochemical models

We applied two global biogeochemical models with increased complexity, the N and N-DOP model (Kriest, Khatiwala, and Oschlies 2010; Piwonski and Slawig 2016). In the following, we briefly introduce these models. For a detailed description of the modeled processes and model equations, we refer to Kriest, Khatiwala, and Oschlies (2010) and Piwonski and Slawig (2016).

The light intensity affects the biogeochemical processes in the ocean. The light limitation function  $I : \Omega \times [0, 1] \rightarrow \mathbb{R}_{\geq 0}$  models the light intensity depending on the insolation. This is based on the astronomical formula of Paltridge and Platt (1976) and considers the ice cover as well as the exponential attenuation of water. According to the light intensity, the ocean is divided into a euphotic (sun lit) zone of about 100 m and an aphotic zone below. A fast and dynamic turnover of phosphorus, especially, is part of the euphotic zone, for instance via photosynthesis, grazing or mortality. Furthermore, a part of the biological production sinks from the euphotic zone as a particulate matter to depth and remineralizes there according to the empirical power-law relationship (Martin et al. 1987).

Table 1: Model parameters of the biogeochemical models.

Parameter	Description	Unit
$k_w$	Attenuation coefficient of water	$\text{m}^{-1}$
$\mu_P$	Maximum growth rate	$\text{d}^{-1}$
$K_N$	Half saturation constant for $\text{PO}_4$ uptake	$\text{mmol P m}^{-3}$
$K_I$	Light intensity compensation	$\text{W m}^{-2}$
$\sigma_{\text{DOP}}$	Fraction of phytoplankton losses assigned to DOP	1
$\lambda'_{\text{DOP}}$	Decay rate	$\text{yr}^{-1}$
$b$	Implicit representation of sinking speed	1

The N model contains only one tracer describing phosphate ( $\text{PO}_4$ ) as inorganic nutrients (cf. Bacastow and Maier-Reimer 1990; Kriest, Khatiwala, and Oschlies 2010). We denote this model as N model (N for nutrients), i.e.,  $\mathbf{y} = (\mathbf{y}_N)$ . The  $n_u = 5$  model parameters  $\mathbf{u} = (k_w, \mu_P, K_N, K_I, b)$  (see Table 1) control the biogeochemical processes. The phytoplankton production (or biological uptake) is defined as

$$f_P : \Omega \times [0, 1] \rightarrow \mathbb{R}, f_P(x, t) = \mu_P y_P^* \frac{I(x, t)}{K_I + I(x, t)} \frac{\mathbf{y}_N(x, t)}{K_N + \mathbf{y}_N(x, t)} \quad (7)$$

and depends on available nutrients and light. Moreover, the uptake of nutrients by phytoplankton is limited using a half saturation function, and applies a model parameter  $\mu_P$  for the maximum production rate as well as a prescribed concentration of phytoplankton  $y_P^* = 0.0028 \text{ mmol P m}^{-3}$ .

Additional to nutrients (N), the N-DOP model includes dissolved organic phosphorus (DOP) (cf. Bacastow and Maier-Reimer 1991; Parekh, Follows, and Boyle 2005; Kriest, Khatiwala, and Oschlies 2010), i.e.,  $\mathbf{y} = (\mathbf{y}_N, \mathbf{y}_{\text{DOP}})$ . Using the same phytoplankton production (7) as the N model, the N-DOP contains  $n_u = 7$  model parameters  $\mathbf{u} = (k_w, \mu_P, K_N, K_I, \sigma_{\text{DOP}}, \lambda'_{\text{DOP}}, b)$  (see Table 1) to describe the internal processes.

### 2.3 Transport matrix method

The *transport matrix method* (TMM) efficiently approximates the tracer transport by matrix-vector multiplications (Khatiwala, Visbeck, and Cane 2005; Khatiwala 2007). Instead of implementing directly a discretization scheme for the advection and diffusion operators  $A$  and  $D$ , the TMM approximates the ocean circulation by matrices because the application of the two operators on a spatially discretized tracer vector is linear and, therefore, the discretized advection-diffusion equation can be written as a linear matrix equation. For this purpose, the TMM computes and stores the matrices obtained by applying the discretized operators on a discrete tracer vector. Consequently, the matrices contain the transport of all parameterized processes represented in the underlying ocean circulation model (Khatiwala, Visbeck, and Cane 2005).

The TMM reduces a time step of the simulation of a marine ecosystem model to matrix-vector multiplications and an evaluation of the biogeochemical model. We assume

that, firstly, the grid with  $n_x \in \mathbb{N}$  grid points  $(x_k)_{k=1}^{n_x}$  is a spatial discretization of the domain  $\Omega$  (i.e., the ocean) and, secondly, the time steps  $t_0, \dots, t_{n_t} \in [0, 1]$ ,  $n_t \in \mathbb{N}$ , specified by

$$t_j := j\Delta t, \quad j = 0, \dots, n_t, \quad \Delta t := \frac{1}{n_t},$$

define an equidistant grid of the time interval  $[0, 1]$  (i.e., one model year). For the time instant  $t_j$ ,  $j \in \{0, \dots, n_t - 1\}$ , the vector  $\mathbf{y}_j := (\mathbf{y}_{ji})_{i=1}^{n_y} \in \mathbb{R}^{n_y n_x}$  combines the numerical approximations for all tracers at time instant  $t_j$  using a reasonable concatenation whereby vector

$$\mathbf{y}_{ji} \approx (y_i(t_j, x_k))_{k=1}^{n_x} \in \mathbb{R}^{n_x}$$

denotes the approximation of the spatially discrete tracer  $y_i$ ,  $i \in \{1, \dots, n_y\}$ . Analogously,

$$\mathbf{q}_{ji} \approx (q_i(x_k, t_j, \mathbf{y}_j, \mathbf{u}))_{k=1}^{n_x} \in \mathbb{R}^{n_x}$$

contains the spatially discretized biogeochemical term of tracer  $y_i$ ,  $i \in \{1, \dots, n_y\}$ , at time instant  $t_j$ ,  $j \in \{0, \dots, n_t - 1\}$ , and  $\mathbf{q}_j := (\mathbf{q}_{ji})_{i=1}^{n_y}$  summarizes this for all tracers at time instant  $t_j$ . In equation (1), we discretize the advection and the horizontal diffusion explicitly and the vertical diffusion implicitly. Using the spatially discrete counterparts  $\mathbf{A}_j$ ,  $\mathbf{D}_j^h$  and  $\mathbf{D}_j^v$  of the operators  $A$ ,  $D_h$  and  $D_v$  at time instant  $t_j$ ,  $j \in \{0, \dots, n_t - 1\}$ , the semi-implicit Euler scheme of (1) results in a time-stepping

$$\mathbf{y}_{j+1} = (\mathbf{I} + \Delta t \mathbf{A}_j + \Delta t \mathbf{D}_j^h) \mathbf{y}_j + \Delta t \mathbf{D}_j^v \mathbf{y}_{j+1} + \Delta t \mathbf{q}_j(\mathbf{y}_j, \mathbf{u}), \quad j = 0, \dots, n_t - 1$$

with the identity matrix  $\mathbf{I} \in \mathbb{R}^{n_x \times n_x}$ . Defining the explicit and implicit transport matrices

$$\begin{aligned} \mathbf{T}_j^{\text{exp}} &:= \mathbf{I} + \Delta t \mathbf{A}_j + \Delta t \mathbf{D}_j^h \in \mathbb{R}^{n_x \times n_x}, \\ \mathbf{T}_j^{\text{imp}} &:= (\mathbf{I} - \Delta t \mathbf{D}_j^v)^{-1} \in \mathbb{R}^{n_x \times n_x} \end{aligned}$$

for each time instant  $t_j$ ,  $j \in \{0, \dots, n_t - 1\}$ , we obtain for a time step of the marine ecosystem model using the TMM

$$\mathbf{y}_{j+1} = \mathbf{T}_j^{\text{imp}} \left( \mathbf{T}_j^{\text{exp}} \mathbf{y}_j + \Delta t \mathbf{q}_j(\mathbf{y}_j, \mathbf{u}) \right) =: \varphi_j(\mathbf{y}_j, \mathbf{u}), \quad j = 0, \dots, n_t - 1. \quad (8)$$

The transport matrices are sparse representations of the monthly averaged tracer transport. The explicit and implicit transport matrices are sparse because these matrices are generated with a grid-point based ocean circulation model and the implicit ones (i.e., the inverse of the discretization matrices) contain only the vertical part of the diffusion. In practical computations, monthly averaged matrices are stored and interpolated linearly to compute an approximation for any time instant  $t_j$ ,  $j = 0, \dots, n_t - 1$ ,

because storing the matrices for all time-steps in a year is practically impossible. Assuming annual periodicity of the ocean circulation, the TMM approximates the ocean circulation using twelve pairs of pre-computed transport matrices. In the present paper, these matrices are computed with the MIT ocean model (Marshall et al. 1997) using a global configuration with a latitudinal and longitudinal resolution of  $2.8125^\circ$  and 15 vertical layers.

## 2.4 Computation of steady annual cycles

A periodic solution (i.e., a steady annual cycle) in a fully discrete setting fulfills

$$\mathbf{y}_{n_t} = \mathbf{y}_0$$

applying the above iteration (8) over one year model time. The nonlinear mapping

$$\Phi := \varphi_{n_t-1} \circ \dots \circ \varphi_0$$

with  $\varphi_j$  specified in (8) defines the time integration of (8) over one model year. For a marine ecosystem model, the steady annual cycle, in particular, is a fixed-point of this mapping. Starting from an arbitrary vector  $\mathbf{y}^0 \in \mathbb{R}^{n_y n_x}$  and model parameters  $\mathbf{u} \in \mathbb{R}^{n_u}$ , a classical fixed-point iteration takes the form

$$\mathbf{y}^{\ell+1} = \Phi(\mathbf{y}^\ell, \mathbf{u}), \quad \ell = 0, 1, \dots \quad (9)$$

The vector  $\mathbf{y}^\ell \in \mathbb{R}^{n_y n_x}$  contains the tracer concentrations at the first time instant of the model year  $\ell \in \mathbb{N}$  if we interpret the fixed-point iteration (9) as pseudo-time stepping or *spin-up*, a term which is widely used in ocean and climate research.

As high-fidelity model, we used  $n_{f,\ell} := 3000$  model years to compute the steady annual cycle with the spin-up. The accuracy of the spin-up is already satisfactory after 3000 model years (Prieß, Piwonski, et al. 2013; Kriest, Khatiwala, and Oschlies 2010). Nevertheless, the spin-up over more than 3000 model years can improve the accuracy. The vector

$$\mathbf{y}_f \approx \left( \mathbf{y}_k^\ell \right)_{k=0, \dots, n_t-1} \in \mathbb{R}^{n_t n_y n_x}$$

contains the trajectory of the steady annual cycle computed with the high-fidelity model and includes the different tracer concentrations  $\mathbf{y}_k^\ell := \varphi_{k-1} \circ \dots \circ \varphi_0(\mathbf{y}^\ell, \mathbf{u})$ , for  $k \in \{1, \dots, n_t - 1\}$ , and  $\mathbf{y}_0^\ell := \mathbf{y}^\ell$  for each time step in the model year.

## 3 The artificial neural network

We applied the prediction of an ANN as an approximation of the steady annual cycle of the N model (Pfeil and Slawig 2021a). For this purpose, we used a multilayer perceptron with a feed-forward architecture consisting of an input layer, three hidden layers and an

output layer. More specifically, we employed a fully connected network, i.e., there do exist all possible connections between the neurons in two consecutive layers.

The ANN predicted the tracer concentration for the first time of the model year using the  $n_u = 5$  model parameters as input. Therefore, the input layer consisted of 5 neurons, while the output layer contained 52 749 neurons. A prediction of the steady annual cycle taking the whole trajectory into account was not possible because the output layer would consist of almost 2.4 million neurons so that the training of the ANN would be infeasible. The fully connected network consisted of three hidden layers with 10, 25 and 211 neurons, respectively.

We trained the ANN with supervised learning (Hastie, Tibshirani, and Friedman 2009) using backpropagation and used the stochastic gradient descent (Rumelhart, G. E. Hinton, and Williams 1986; Bottou and Bousquet 2008) for the optimization of the network weights. The loss function was the mean squared error. For the neurons of the hidden layers, we applied the exponential linear unit (Clevert, Unterthiner, and Hochreiter 2015) as activation function and the scaled exponential linear unit (Klambauer et al. 2017) for the neurons of the output layer.

The total mass of the predicted tracer concentration was essential for a reasonable prediction because the marine ecosystem model preserves mass. We adjusted the prediction  $\mathbf{y}_{\text{ANN}} \in \mathbb{R}^{n_x}$  of the ANN pointwise by

$$\tilde{\mathbf{y}}_{\text{ANN}} = \frac{\sum_{k=1}^{n_x} |V_k| m}{\sum_{k=1}^{n_x} |V_k| \mathbf{y}_{\text{ANN}}(x_k, t_0)} \mathbf{y}_{\text{ANN}}$$

using the box volumes  $|V_k|$ ,  $k = 1, \dots, n_x$ , of the discretization and a global mean tracer concentration  $m \in \mathbb{R}_{>0}$  in order to obtain the required overall mass.

A given set of pairs of input and output data is divided into *training*, *validation* and *test data* for the training procedure (i.e., the optimization of the internal weights of the ANN) using supervised learning. The optimization adjusts the internal weights by the use of the training data and monitors the behavior of the already partially optimized network on the validation data. The test data are used to assess the quality of the trained network after finishing the training procedure.

## 4 Surrogate-based optimization

The SBO (Bandler et al. 2004; Queipo et al. 2005; Forrester and Keane 2009; Leifsson and Koziel 2010) replaces the high-fidelity model by a surrogate during the optimization. For many nonlinear optimization problems, the high computational effort to evaluate the objective function is a major bottleneck. Conversely, the SBO uses the surrogate to reduce the computational effort because the evaluation of the surrogate is computationally much cheaper and still represents a reasonable approximation of the high-fidelity model. In order to obtain optimal model parameters close to the high-fidelity optimum, the SBO keeps the surrogate close to the high-fidelity model by iterative updates and re-optimization of the surrogate. As a result, the calculated parameters of a well performing SBO are close to those of a conventional optimization algorithm.

## 4.1 Cost function

For the optimization, we defined the discrete cost function

$$J(\mathbf{z}) := \frac{1}{2} \|\mathbf{z} - \mathbf{y}_d\|_2^2 := \frac{1}{2} \sum_{j=0}^{n_t-1} \sum_{i=1}^{n_y} \sum_{k=1}^{n_x} (z_{jik} - y_{d,jik})^2 \quad (10)$$

by measuring the difference between an annual cycle  $\mathbf{z} \in \mathbb{R}^{n_t n_y n_x}$ , for example calculated during the optimization process, and the target annual cycle  $\mathbf{y}_d \in \mathbb{R}^{n_t n_y n_x}$  in an Euclidean norm. Both vectors  $\mathbf{z}$  and  $\mathbf{y}_d$  are indexed as  $\mathbf{z} = \left( (z_{jik})_{k=1}^{n_x} \right)_{i=1}^{n_y} \Big)_{j=0}^{n_t-1}$  and  $\mathbf{y}_d = \left( (y_{jik})_{k=1}^{n_x} \right)_{i=1}^{n_y} \Big)_{j=0}^{n_t-1}$ . We did not use weights in the Euclidean norm because we performed the following optimizations exclusively with synthetic data. When using real measurement data, the cost function (10) can be restricted by weights, for example, to take only discrete points in space and time for which measurements exist or the error variances of the measurements into account. In addition, the cost function can be restricted to individual tracers. Kriest, Khatiwala, and Oschlies (2010) investigated different cost functions for biogeochemical models.

## 4.2 Optimization

We used the SBO instead of a conventional optimization approach (for example gradient-based or meta-heuristics) to identify the optimal parameters of a biogeochemical model. These parameters are usually identified using a nonlinear optimization problem

$$\min_{\mathbf{u} \in U_{ad}} J(\mathbf{y}_f(\mathbf{u}))$$

with the set of admissible parameters  $U_{ad} := \{\mathbf{u} \in \mathbb{R}^{n_u} : \mathbf{b}_\ell \leq \mathbf{u} \leq \mathbf{b}_u\}$  and parameter boundaries  $\mathbf{b}_\ell, \mathbf{b}_u \in \mathbb{R}^{n_u}$  with  $\mathbf{b}_\ell \leq \mathbf{b}_u$ . The inequalities with the parameter boundaries are meant component-wise. We did not optimize the expensive high-fidelity model ( $\mathbf{y}_f$ ) using any conventional approach because the computational effort is unaffordable.

The SBO replaces the high-fidelity model with its surrogate, whose evaluation is computationally cheaper than the high-fidelity model but still provides a reasonably accurate approximation of the high-fidelity model. There are several ways of constructing the surrogate, such as *function-approximation* surrogates (Queipo et al. 2005; Simpson et al. 2001; Smola and Schölkopf 2004) or *physically-based* surrogates (Søndergaard 2003). In the present paper, we used two different methods to construct the low-fidelity model ( $\mathbf{y}_c$ ): a physics-based low-fidelity model and a neural network. These low-fidelity models are a less accurate but computationally more efficient approximation of the high-fidelity model. However, the accuracy of the low-fidelity models is not sufficient for a direct optimization. In order to reduce the misalignment with respect to the high-fidelity model, we form the surrogate from the low-fidelity model with a subsequent correction. Since the surrogate approximates only the high-fidelity model adequately in a local environment, we also used a trust-region safeguard (Conn, Gould, and Toint 2000; Koziel, Bandler, and Cheng 2010; Prieß, Piwonski, et al. 2013) to limit the step size in the optimization to

---

 Algorithm 1: Surrogate-based optimization
 

---

**Data:**  $\mathbf{u}_0 \in \mathbb{R}^{n_u}$ ,  $\delta_0 \in \mathbb{R}_{>0}$ ,  $\delta^{\min} \in \mathbb{R}_{>0}$ ,  $\gamma \in \mathbb{R}_{>0}$ ,  $r_{\text{decr}} \in \mathbb{R}_{>0}$ ,  $r_{\text{incr}} \in \mathbb{R}_{>0}$ ,  
 $m_{\text{decr}} \in \mathbb{R}_{>0}$ ,  $m_{\text{incr}} \in \mathbb{R}_{>0}$ ,  $a_\ell \in \mathbb{R}_{>0}$ ,  $a_u \in \mathbb{R}_{>0}$ ,  $\delta \in \mathbb{R}_{>0}$ ,  
**Result:**  $\mathbf{u}_{k_{\min}} \in \mathbb{R}^{n_u}$  with  $k_{\min} = \min \left\{ k \in \mathbb{N} : \|\mathbf{u}_k - \mathbf{u}_{k-1}\|_2^2 \leq \gamma \vee \delta_k \leq \delta_k^{\min} \right\}$

$k = 0$   
**while**  $k = 0 \vee \|\mathbf{u}_k - \mathbf{u}_{k-1}\|_2^2 \leq \gamma \vee \delta_k \leq \delta^{\min}$  **do**  
     Evaluate high-fidelity  $\mathbf{y}_f(\mathbf{u}_k)$  and low-fidelity model  $\mathbf{y}_c(\mathbf{u}_k)$   
     // Construct surrogate  
     Compute correction vector  $\mathbf{a}_k \in \mathbb{R}^{n_t n_y n_x}$  with
 
$$a_{k,jil} := \begin{cases} 1.0, & (\mathbf{y}_f(\mathbf{u}_k))_{jil} < \delta \vee (\mathbf{y}_c(\mathbf{u}_k))_{jil} < \delta \\ a_\ell, & \frac{(\mathbf{y}_f(\mathbf{u}_k))_{jil}}{(\mathbf{y}_c(\mathbf{u}_k))_{jil}} < a_\ell \\ a_u, & \frac{(\mathbf{y}_f(\mathbf{u}_k))_{jil}}{(\mathbf{y}_c(\mathbf{u}_k))_{jil}} > a_u \\ \frac{(\mathbf{y}_f(\mathbf{u}_k))_{jil}}{(\mathbf{y}_c(\mathbf{u}_k))_{jil}}, & \text{else} \end{cases},$$
  
 $i \in \{1, \dots, n_y\}, j \in \{0, \dots, n_t - 1\}, l \in \{1, \dots, n_x\}$   
      $\mathbf{s}_k(\mathbf{u}) := \mathbf{a}_k \mathbf{y}_c(\mathbf{u})$   
     // Optimize surrogate  
      $\mathbf{u}_{k+1} = \operatorname{argmin}_{\mathbf{u} \in U_{ab}, \|\mathbf{u} - \mathbf{u}_k\|_2 \leq \delta_k} J(\mathbf{s}_k(\mathbf{u}))$   
     // Update trust-region radius  
     **if**  $J(\mathbf{y}_f(\mathbf{u}_{k+1})) < J(\mathbf{y}_f(\mathbf{u}_k))$  **then**  
          $\rho_k = \frac{J(\mathbf{y}_f(\mathbf{u}_{k+1})) - J(\mathbf{y}_f(\mathbf{u}_k))}{J(\mathbf{s}_k(\mathbf{u}_{k+1})) - J(\mathbf{s}_k(\mathbf{u}_k))}$   
          $\delta_{k+1} = \begin{cases} \frac{\delta_k}{m_{\text{decr}}}, & \rho_k < r_{\text{decr}}, \\ \delta_k, & r_{\text{decr}} \leq \rho_k \leq r_{\text{incr}} \\ \delta_k \cdot m_{\text{incr}}, & \rho_k > r_{\text{incr}} \end{cases}$   
          $k = k + 1$   
     **else**  
          $\delta_k = \frac{\delta_k}{m_{\text{decr}}}$

---

a certain trusted region ensuring the computation of a local minimum with the surrogate if both the low- and the high-fidelity model are sufficiently smooth. This enhances any surrogate optimization.

The SBO consists of an iterative approach generating the surrogate again after a successful surrogate optimization. The algorithm of the SBO shown in Algorithm 1 can be divided into three parts. The first part contains the evaluation of the low- and high-fidelity model including the construction of the surrogate. The different low-fidelity models used in this paper are explained in Section 4.2.1, 4.2.2 as well as 4.2.3, and the construction of the surrogate as a correction of the low-fidelity model is presented in Section 4.2.4. In the second part of the algorithm, the surrogate ( $\mathbf{s}_k$ ) is optimized using

a gradient-based algorithm, i.e.,

$$\mathbf{u}_{k+1} = \underset{\mathbf{u} \in U_{ad}, \|\mathbf{u} - \mathbf{u}_k\| \leq \delta_k}{\operatorname{argmin}} J(\mathbf{s}_k(\mathbf{u}))$$

for the iteration  $k \in \mathbb{N}_0$  and trust-region radius  $\delta_k \in \mathbb{R}_{>0}$ . If the surrogate optimization reduces the cost function value evaluated for the high-fidelity model, the parameter vector  $\mathbf{u}_{k+1}$  is accepted and the trust-region radius is updated according to the rules below. Otherwise, the parameter vector  $\mathbf{u}_{k+1}$  is rejected, and the surrogate optimization is performed again with the same surrogate but reduced trust-region radius. In analogy to Prieß, Piwonski, et al. (2013), we used the classical rules for updating the trust-region radius (Conn, Gould, and Toint 2000; Koziel, Bandler, and Cheng 2010) with slightly modified parameters, i.e.,

$$\delta_{k+1} = \begin{cases} \frac{\delta_k}{m_{\text{decr}}}, & \rho_k < r_{\text{decr}} \\ \delta_k, & r_{\text{decr}} \leq \rho_k \leq r_{\text{incr}} \\ \delta_k \cdot m_{\text{incr}}, & \rho_k > r_{\text{incr}} \end{cases}$$

with the parameters  $\delta_0 = 0.06$ ,  $r_{\text{incr}} = 0.75$ ,  $r_{\text{decr}} = 0.01$  and  $m_{\text{incr}}, m_{\text{decr}} \in \mathbb{R}_{>0}$  as well as the gain ratio

$$\rho_k := \frac{J(\mathbf{y}_f(\mathbf{u}_{k+1})) - J(\mathbf{y}_f(\mathbf{u}_k))}{J(\mathbf{s}_k(\mathbf{u}_{k+1})) - J(\mathbf{s}_k(\mathbf{u}_k))}.$$

Consequently, the trust-region radius is decreased, on the one hand, if the parameter vector  $\mathbf{u}_{k+1}$  is rejected, or if the improvement of the cost function value which was evaluated with the high-fidelity model is too small compared to the prediction by the surrogate and increased, on the other hand, if the prediction by the surrogate was adequate. The termination condition of the iterative approach represents the third part of the algorithm. We used a threshold  $\gamma \in \mathbb{R}_{>0}$  for the absolute step size in combination with a threshold  $\delta^{\text{min}} \in \mathbb{R}_{>0}$  for the trust-region radius. Alternative termination conditions, for example, are certain convergence criteria, an expected cost function value or a specific number of iterations.

#### 4.2.1 Low-fidelity model using truncated spin-up

Our first low-fidelity model used the approach of a truncated spin-up (denoted as  $\mathbf{y}_c^{\text{N-DOP}}$  for the N-DOP model and  $\mathbf{y}_c^{\text{N}}$  for the N model) (Prieß, Piwonski, et al. 2013). In order to compute an approximation of the steady annual cycle using the low-fidelity model, we reduced the number of model years to  $n_c = 25$  (cf. Section 2.4). The time steps were, however, identical for the low- and high-fidelity model. The number of model years  $n_f = 3000$  employed for the spin-up calculation of the high-fidelity model is much larger than  $n_c$  for the low-fidelity model. Therefore, the computational effort for the low-fidelity model is significantly lower than for the high-fidelity model.

#### 4.2.2 Low-fidelity model using prediction of an ANN

Our second low-fidelity model approximated the steady annual cycle with the prediction of an ANN (Pfeil and Slawig 2021a). For this purpose, the ANN predicted the tracer concentration of a steady annual cycle approximation for the first time of the model year. To receive the whole trajectory as low-fidelity model (denoted as  $\mathbf{y}_c^{\text{ANN}}$ ), we calculated the spin-up over one model year using the prediction as initial concentration. We used the ANN described in Section 3 including the adjustment of the prediction to obtain the required overall mass. Particularly, the computational effort to evaluate this low-fidelity model is very low because the computation of the trajectory for one model year is already the main effort.

#### 4.2.3 Low-fidelity model using ANN as initial value generator

For our third low-fidelity model, the prediction of the ANN served as initial concentration for a truncated spin-up (Pfeil and Slawig 2021a). Instead of using the prediction directly as low-fidelity model as in Section 4.2.2, we used the ANN described in Section 3 to generate an initial concentration for the spin-up calculation with a reduced number of model years  $n_c = 50$ . The time step was the same as for the high-fidelity model. In summary, the low-fidelity (denoted as  $\mathbf{y}_c^{\text{ANN-N}}$ ) model consisted of the ANN as initial value generator in combination with a truncated spin-up. This low-fidelity model reduced again the computationally effort with respect to the high-fidelity model.

#### 4.2.4 Multiplicative response correction

For the three low-fidelity models, the multiplicative response correction reduces the misalignment of the low-fidelity model with respect to the high-fidelity model. Prieß, Koziel, and Slawig (2011) and Prieß, Piwonski, et al. (2013) have already used this multiplicative correction motivated by the physics-based approach of the low-fidelity model because the steady annual cycle calculated with the low-fidelity model resembles that of the high-fidelity model. For each iteration  $k \in \mathbb{N}_0$ , the multiplicative correction vector  $\mathbf{a}_k \in \mathbb{R}^{n_t n_y n_x}$  contains the pointwise ratio of the high- and low-fidelity solution

$$\mathbf{a}_k := \frac{\mathbf{y}_f(\mathbf{u}_k)}{\mathbf{y}_c(\mathbf{u}_k)}.$$

In order to avoid larger entries in the correction vector, for example for values of the low-fidelity model close to zero or for a value of the low-fidelity model being several orders of magnitude smaller than the value of the high-fidelity model, we restrict the entries of the correction vector by an upper bound ( $a_u \in \mathbb{R}_{>0}$ ) and a lower one ( $a_\ell \in \mathbb{R}_{>0}$ ) and, furthermore, we set the value to 1.0 if the value of the low-fidelity model or high-fidelity model is close to zero, i.e., falls below a threshold of  $\delta = 5 \cdot 10^{-3}$ . The pointwise multiplication of the correction vector  $\mathbf{a}_k$  and the low-fidelity solution defines the surrogate, i.e.,

$$\mathbf{s}_k(\mathbf{u}) := \mathbf{a}_k \mathbf{y}_c(\mathbf{u})$$

Table 2: Parameter vectors for the biogeochemical models. Initial ( $\mathbf{u}_0$ ) and optimal ( $\mathbf{u}_d$ ) parameter vector used for the SBO runs, test parameter vector ( $\bar{\mathbf{u}}$  and  $\tilde{\mathbf{u}}$ ) to assess the quality of the surrogate model as well as lower ( $\mathbf{b}_\ell$ ) and upper ( $\mathbf{b}_u$ ) bounds for the parameter vectors.

Parameter	$k_w$	$\mu_P$	$K_N$	$K_I$	$\sigma_{\text{DOP}}$	$\lambda'_{\text{DOP}}$	$b$
$\mathbf{u}_0$	0.04	3.5	0.8	25.0	0.4	0.3	0.78
$\mathbf{u}_d$	0.02	2.0	0.5	30.0	0.67	0.5	0.858
$\bar{\mathbf{u}}$	0.016	1.6	0.4	24.0	0.536	0.4	0.686
$\tilde{\mathbf{u}}$	0.0193	1.93	0.483	29.0	0.648	0.483	0.829
$\mathbf{b}_\ell$	0.01	1.0	0.25	15.0	0.05	0.25	0.7
$\mathbf{b}_u$	0.05	4.0	1.0	60.0	0.95	1.0	1.5

for  $\mathbf{u} \in U_{ad}$ . In particular, the construction of the surrogate exclusively requires a single evaluation of the high-fidelity model. The subsequent optimization needs only the evaluation of the surrogate and thus of the low-fidelity model. Moreover, this construction of the surrogate improves its accuracy and the performance of the entire SBO (Prieß, Piwonski, et al. 2013).

## 5 Results

We present in this section the results obtained with the three different low-fidelity models. For the low-fidelity model described in Section 4.2.1, we performed a parameter optimization for both biogeochemical models. In contrast, we used the low-fidelity models described in Section 4.2.2 and 4.2.3 only for a parameter optimization using the N model because the neural network in Section 3 was designed for the N model. In this paper, we have used synthetic target data for the parameter optimization in order to compare the different low-fidelity models. We assessed the optimization, on the one hand, with the improvement of the cost function  $J(\mathbf{y}_f)$  and, on the other hand, using the accuracy of matching both the target phosphate concentration and the optimal parameters.

### 5.1 Experimental setup

We configured the surrogate-based optimization uniformly for each low-fidelity model. Although Table 2 lists the parameter vectors exclusively for the N-DOP model, we used these parameter vectors also for the N model. For this purpose, the parameter vector  $(k_w, \mu_P, K_N, K_I, \sigma_{\text{DOP}}, \lambda'_{\text{DOP}}, b)$  of the N-DOP model had to be restricted to the parameter vector  $(k_w, \mu_P, K_N, K_I, b)$  of the N model, i.e., the parameters  $\sigma_{\text{DOP}}$  and  $\lambda'_{\text{DOP}}$  were omitted.

### 5.1.1 Training of the ANN

We trained the fully connected network described in Section 3 using the parameter vectors of a Latin hypercube sample (cf. McKay, Beckman, and Conover 1979). We created the Latin hypercube sample with 1100 parameter vectors within the bounds ( $\mathbf{b}_\ell$  and  $\mathbf{b}_u$ ) of Table 2 using the routine LHS of Lee (2014) and computed a steady annual cycle for each parameter vector. For the computation of the steady annual cycle, we applied the marine ecosystem toolkit for optimization and simulation in 3D (Metos3D) (Piwonski and Slawig 2016) and performed a spin-up over 10 000 model years, starting from a global mean concentration of  $2.17 \text{ mmol P m}^{-3}$  for  $\text{PO}_4$ . For the training of the fully connected network, we used the parameter vectors of the Latin hypercube sample as input and the tracer concentration of the first time instant in the last, the 10 000th, model year as output. We trained the neural network over 1000 iterations/epochs.

### 5.1.2 Setup of the surrogate-based optimization

For the calculation of a steady annual cycle, we applied Metos3D using  $n_t = 45$  time steps. Except for the two low-fidelity models using the ANN (see Section 4.2.2 and 4.2.3), the spin-up calculation started always with a constant global mean concentration of  $2.17 \text{ mmol P m}^{-3}$  for  $\text{PO}_4$  and, if present,  $0.0001 \text{ mmol P m}^{-3}$  for DOP. For the synthetic data, we selected a random parameter vector  $\mathbf{u}_d \in \mathbb{R}^{n_u}$  (see Table 2) and computed the steady annual cycle  $\mathbf{y}_d \in \mathbb{R}^{n_t n_y n_x}$  using the spin-up over 10 000 model years with  $n_t = 2880$  time steps and restricted the steady annual cycle to the corresponding time steps for  $n_t = 45$ , i.e.,

$$\mathbf{y}_d := \left( \mathbf{y}_i^{10000}(\mathbf{u}_d) \right)_{i \in \{0, 64, \dots, 2816\}}.$$

The SBO used the L-BFGS-B algorithm as optimization algorithm for the surrogate (Byrd et al. 1995; Zhu et al. 1997) implemented in SciPy<sup>1</sup> (Virtanen et al. 2020). We started the SBO exemplary from a random parameter vector  $\mathbf{u}_0 \in \mathbb{R}^{n_u}$  shown in Table 2. Moreover, we limited the admissible parameter vectors using the lower  $\mathbf{b}_\ell$  and upper bound  $\mathbf{b}_u$  (Table 2). The SBO stopped if the absolute step size fell below a threshold of  $\gamma = 5 \cdot 10^{-4}$ , or the trust-region radius undercut a threshold of  $\delta^{\min} = 5 \cdot 10^{-5}$ . Finally, we restricted the entries of the multiplicative correction vector for each surrogate using the lower and upper bounds  $a_\ell = 0.1$  and  $a_u = 5$ .

## 5.2 Suitability of the multiplicative correction technique

The multiplicative response correction was suitable for the three low-fidelity models. Figure 1 indicates the improvement of the low-fidelity model accuracy using the multiplicative response correction. Although the concentrations of the low-fidelity models differed significantly from each other in some areas, the approximations of the high-fidelity model were very similar after the multiplicative correction. Particularly, the surrogate approximated the high-fidelity model better for each low-fidelity model if the

<sup>1</sup>Scientific computing tools for Python, <https://www.scipy.org>

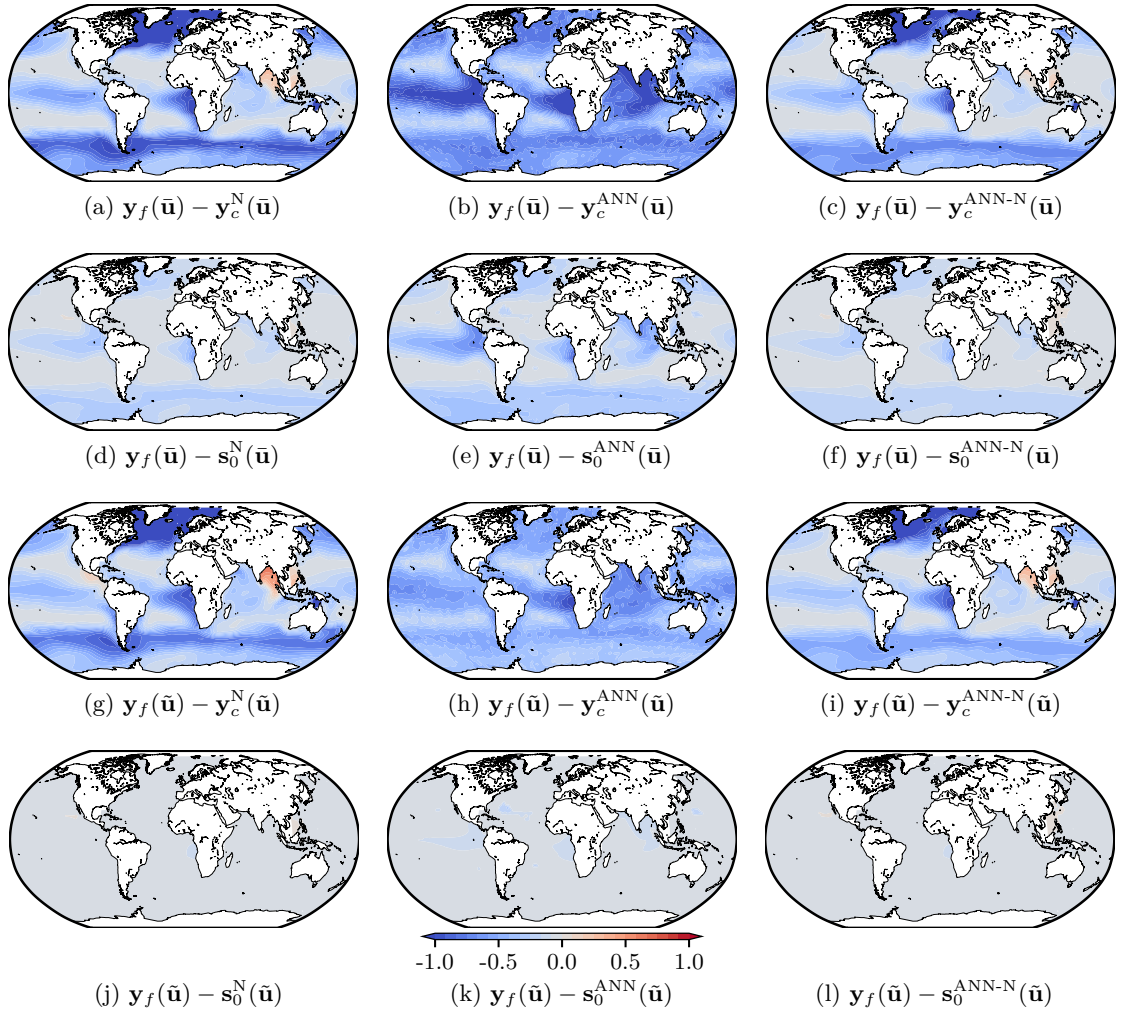


Figure 1: Difference between the high-fidelity model  $\mathbf{y}_f$  and the low-fidelity model  $\mathbf{y}_c$  as well as the surrogate  $\mathbf{s}_0$  for the three different low-fidelity models (truncated-spin-up  $\mathbf{y}_c^N$  (left, Section 4.2.1), ANN prediction  $\mathbf{y}_c^{\text{ANN}}$  (middle, Section 4.2.2) and ANN prediction as initial concentration for the truncated spin-up  $\mathbf{y}_c^{\text{ANN-N}}$  (right, Section 4.2.3) as low-fidelity model). For the two parameter vectors  $\bar{\mathbf{u}}$  and  $\tilde{\mathbf{u}}$ , the phosphate concentration difference are shown on the surface (0 m to 50 m) at the first time step of the model year (in January). The surrogate was built using the parameter vector  $\mathbf{u}_d$ , respectively.

parameter vector was closer to the parameter vector used to construct the surrogate. The approximation was, nevertheless, slightly worse using the prediction of the ANN as low-fidelity model while the other two low-fidelity models showed only marginal differences in the approximations after the correction. Except for the low-fidelity model using the ANN prediction as detailed in Section 5.4, the surrogates provided an appropriate

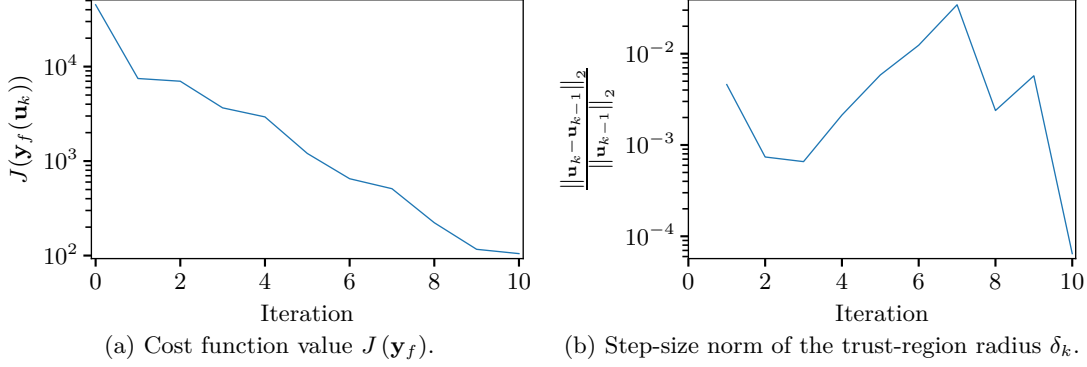


Figure 2: Convergence of the cost function value and the step-size norm of the trust-region radius for the exemplary SBO run with the truncated spin-up as low-fidelity model ( $\mathbf{y}_c^{\text{N-DOP}}$ ) and the N-DOP model.

approximation of the high-fidelity model in the neighborhood of the parameter vector used to construct the surrogate.

### 5.3 Low-fidelity model as truncated spin-up

In this section, we present the parameter identification with the SBO using the low-fidelity model based on the truncated spin-up (see Section 4.2.1) for both biogeochemical models. For the update of the trust-region radius, we applied the parameter  $m_{\text{incr}} = 3$  for both biogeochemical models, as well as the parameter  $m_{\text{decr}} = 20$  for the N-DOP model and  $m_{\text{decr}} = 3$  for the N model.

#### 5.3.1 N-DOP model

The parameter identification using the SBO identified six out of seven model parameters of the N-DOP model. The steady annual cycles calculated for each iteration of the SBO converged to the target concentration  $\mathbf{y}_d$  (Figure 2). Furthermore, the single parameter values converged against the values of the optimal parameter vector  $\mathbf{u}_d$  (see Figure 3), except for parameter  $K_I$ . Especially in the iterations four to eight, the SBO reduced the difference to the optimal parameter vector whereas even the step size increased significantly. The SBO terminated after ten iterations because the step size fell below the threshold of  $\gamma = 5 \cdot 10^{-5}$  (i.e.,  $\|\mathbf{u}_{10} - \mathbf{u}_9\|_2^2 < \gamma$ ). Although the main patterns of the target phosphate concentration are already visible for the solution  $\mathbf{y}_f(\mathbf{u}_0)$  of the initial parameter vector  $\mathbf{u}_0$ , Figures 4 and 5 show the further improvement of the match (for instance in the North Atlantic on the surface layer) during the optimization.

The SBO was computationally very efficient. The exemplary SBO run required only 15 high-fidelity model evaluations, whereby the surrogate optimization of four iterations were discarded due to a larger cost function value after the optimization. In contrast, the surrogate optimization needed altogether more than 6000 evaluations of the surrogate.

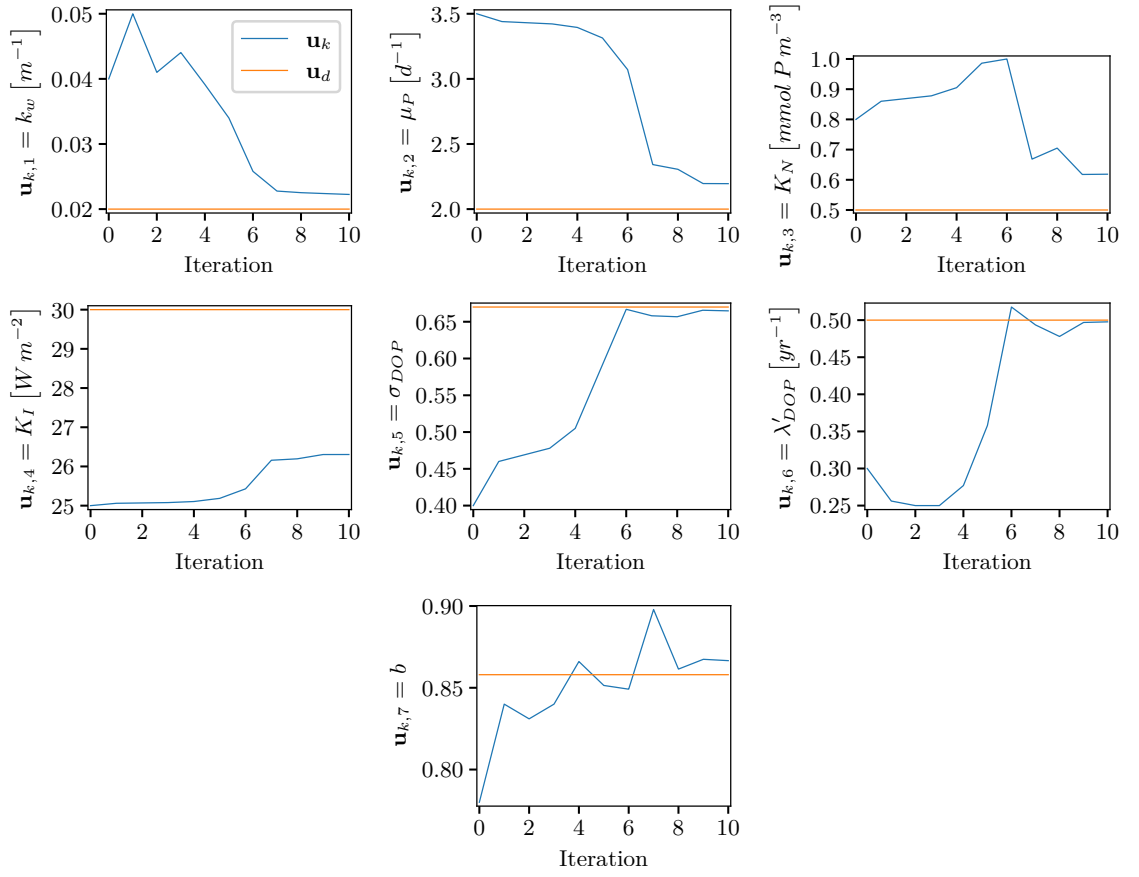


Figure 3: Convergence of the single parameter values  $\mathbf{u}_{k,i}$  for each iteration of the exemplary SBO run with the truncated spin-up as low-fidelity model ( $\mathbf{y}_c^{\text{N-DOP}}$ ) and the N-DOP model.

This large number of surrogate evaluations resulted from the limitation of the iterations of the surrogate optimization to 100. Limiting the number of iterations to 10, the SBO run converged with a cost function value of about 650 (instead of about 100 using a limit of 100 iterations as illustrated by Figure 2a) but with a significantly lower number of about 1500 surrogate evaluations.

### 5.3.2 N model

The parameters converged to the optimal parameter  $\mathbf{u}_d$  using the SBO for the N model with the exception of parameter  $K_I$ . The cost function values  $J(\mathbf{y}_f)$  in Figure 6a indicate a solution close to the target data  $\mathbf{y}_d$ . Particularly, the SBO identified four out of five model parameters as detailed in Figure 7. Although the first iteration already determined the parameter  $b$ , the SBO required twelve iterations to identify the other three parameters. Thereby, the algorithm repeatedly increased the step size (Figure

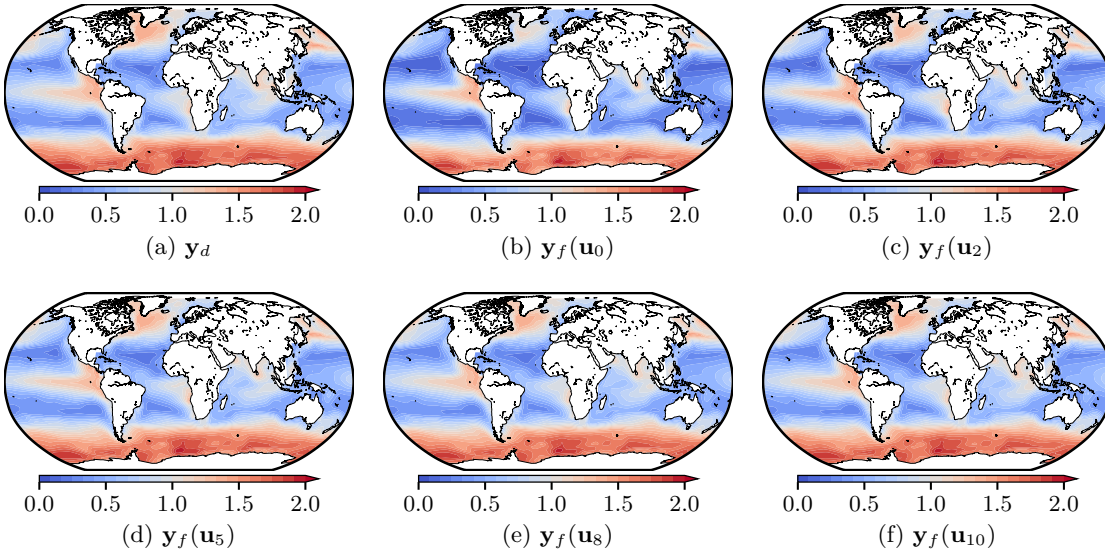


Figure 4: High-fidelity model output  $\mathbf{y}_f$  obtained by the exemplary SBO run with the truncated spin-up as low-fidelity model ( $\mathbf{y}_c^{\text{N-DOP}}$ ) and the N-DOP model at the beginning and after two, five, eight and ten iterations (i.e., evaluated with the parameter vectors  $\mathbf{u}_0$ ,  $\mathbf{u}_2$ ,  $\mathbf{u}_5$ ,  $\mathbf{u}_8$  and  $\mathbf{u}_{10}$ ) as well as the target data  $\mathbf{y}_d$ . Shown are the phosphate concentrations on the surface layer (0 m to 50 m) at the first time step of the model year (in January).

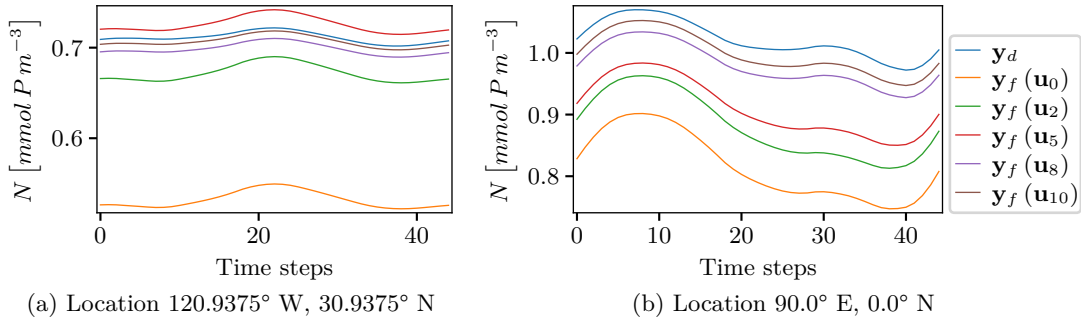


Figure 5: Annual cycles of phosphate of the high-fidelity model output  $\mathbf{y}_f$  obtained by the exemplary SBO run with the truncated spin-up as low-fidelity model ( $\mathbf{y}_c^{\text{N-DOP}}$ ) and the N-DOP model at the beginning and after two, five, eight and ten iterations (i.e., evaluated with the parameter vectors  $\mathbf{u}_0$ ,  $\mathbf{u}_2$ ,  $\mathbf{u}_5$ ,  $\mathbf{u}_8$  and  $\mathbf{u}_{10}$ ) as well as the target data  $\mathbf{y}_d$  on the surface layer (0 m to 50 m) for two distinct locations.

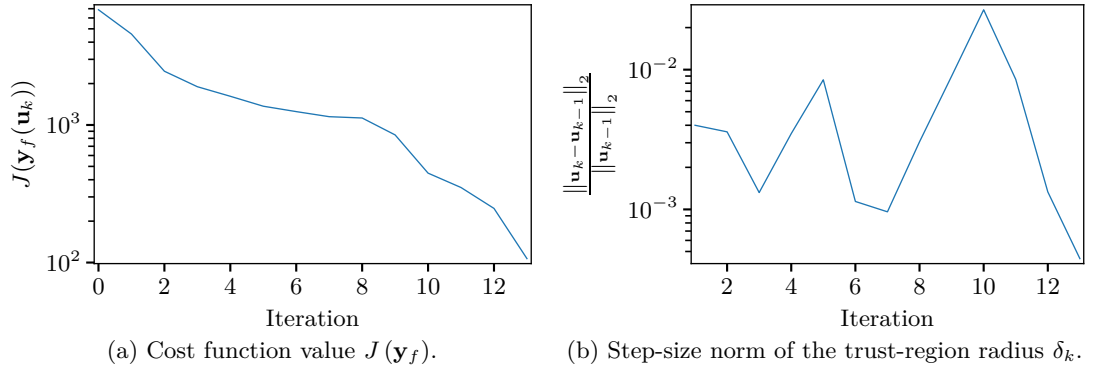


Figure 6: Convergence of the cost function value and the step-size norm of the trust-region radius for the exemplary SBO run with the truncated spin-up as low-fidelity model ( $\mathbf{y}_c^N$ ) and the N model.

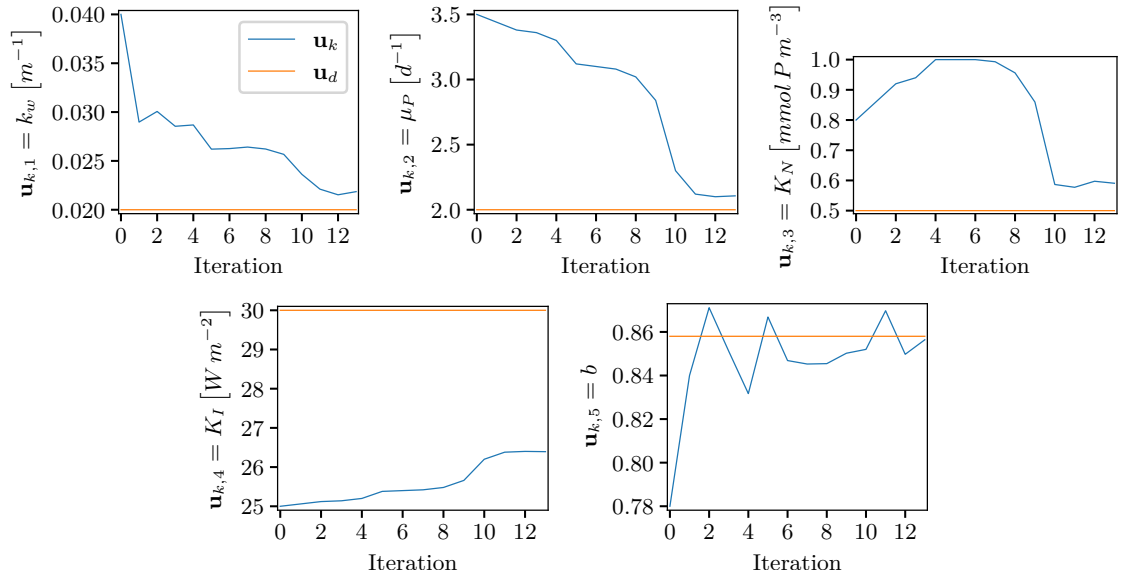


Figure 7: Convergence of the single parameter values  $\mathbf{u}_{k,i}$  for each iteration of the exemplary SBO run with the truncated spin-up as low-fidelity model ( $\mathbf{y}_c^N$ ) and the N model.

6b). As a result of falling below the threshold  $\delta^{\min}$  for the trust-region radius, the SBO terminated after 13 iterations. According to Figures 8 and 9, the main patterns of the target phosphate concentration are apparent for the tracer concentrations of the selected parameter vectors. However, the SBO improved the match sequentially (for example in the Indian Ocean, see also Figure 6a). Nevertheless, local worsening occurred occasionally compared to the previously calculated concentration (cf. Figure 9).

The computational costs of the SBO were low. The exemplary SBO run required only

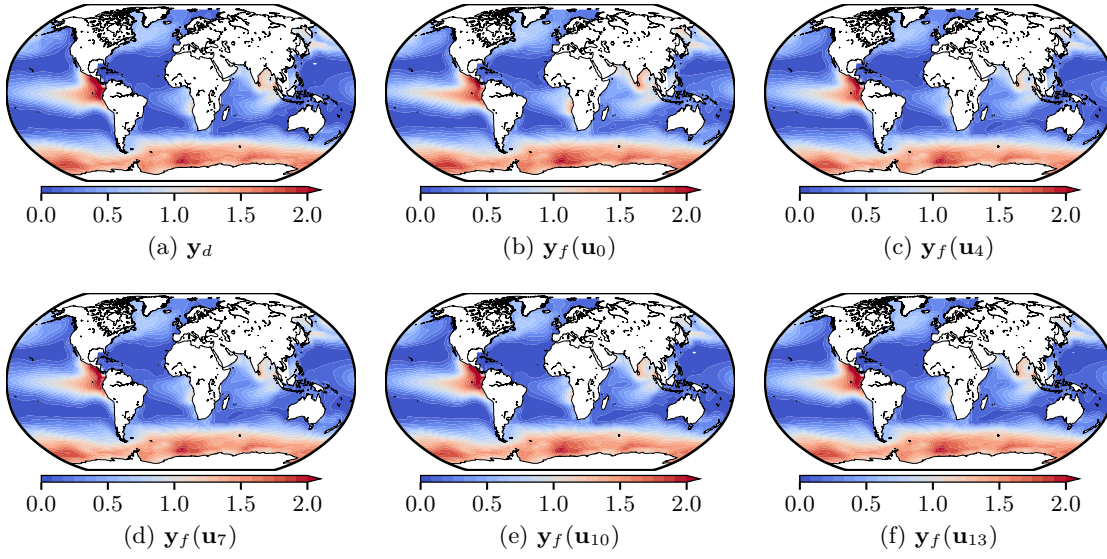


Figure 8: High-fidelity model output  $\mathbf{y}_f$  obtained by the exemplary SBO run with the truncated spin-up as low-fidelity model ( $\mathbf{y}_c^N$ ) and the N model at the beginning and after 4, 7, 10 and 13 iterations (i.e., evaluated with the parameter vectors  $\mathbf{u}_0$ ,  $\mathbf{u}_4$ ,  $\mathbf{u}_7$ ,  $\mathbf{u}_{10}$  and  $\mathbf{u}_{13}$ ) as well as the target data  $\mathbf{y}_d$ . Shown are the phosphate concentrations on the surface layer (0 m to 50 m) at the first time step of the model year (in January).

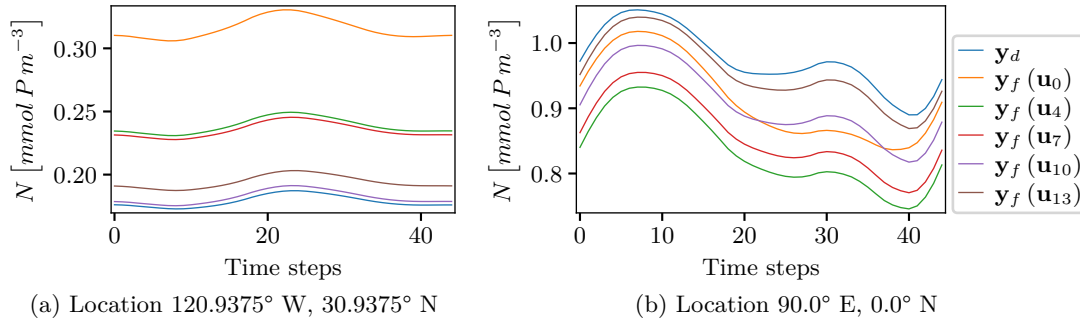


Figure 9: Annual cycles of phosphate of the high-fidelity model output  $\mathbf{y}_f$  obtained by the exemplary SBO run with the truncated spin-up as low-fidelity model ( $\mathbf{y}_c^N$ ) and the N model at the beginning and after 4, 7, 10 and 13 iterations (i.e., evaluated with the parameter vectors  $\mathbf{u}_0$ ,  $\mathbf{u}_4$ ,  $\mathbf{u}_7$ ,  $\mathbf{u}_{10}$  and  $\mathbf{u}_{13}$ ) as well as the target data  $\mathbf{y}_d$  on the surface layer (0 m to 50 m) for two distinct locations.

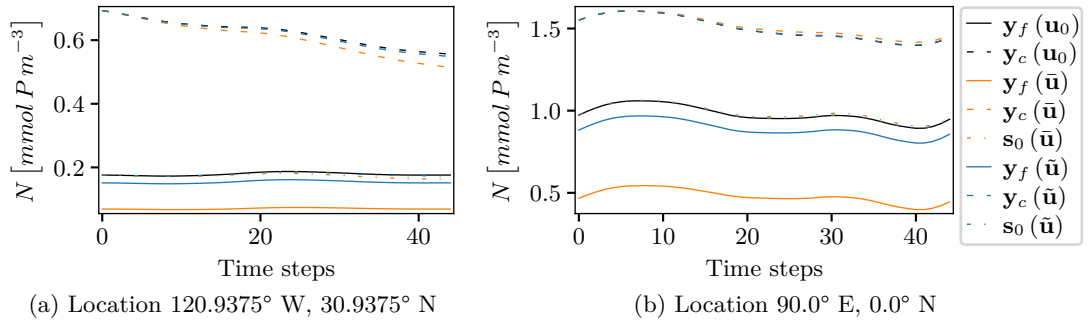


Figure 10: Annual cycle of phosphate for the high- ( $\mathbf{y}_f$ ), low-fidelity model ( $\mathbf{y}_c^{\text{ANN}}$ ) and surrogate ( $\mathbf{s}_0$ ) on the surface layer (0 m to 50 m) for two distinct locations. Shown are the annual cycles for three parameter values  $\mathbf{u}_0$  (as “reference point”),  $\bar{\mathbf{u}}$  (a neighbouring point),  $\tilde{\mathbf{u}}$  (a point in a closer vicinity). The surrogate was built using parameter vector  $\mathbf{u}_0$ , the reason why the solution of the surrogate is omitted at the reference point.

34 high-fidelity model evaluations and about 6000 surrogate evaluations. Compared to the small number of 13 iterations, more than half of the high-fidelity model evaluations resulted from the calculation of the reference cost function value for parameter vectors that had been calculated by the surrogate optimization but did not cause a reduction of the cost function. Analogous to the SBO using the N-DOP model in the previous section 5.3.1, the number of surrogate evaluations could be reduced by limiting the optimization iterations of the surrogate optimization to 10. As a consequence, the final cost function value increased significantly to over 1000 for such an optimization run compared to a value of about 100 when a limit of 100 iterations of the surrogate optimization was used as shown in Figure 6a.

#### 5.4 Prediction of an ANN as low-fidelity model

Using the prediction of the ANN defined in Section 3 as low-fidelity model (see Section 4.2.2) was unsuitable to construct a reliable surrogate in conjunction with the multiplicative response correction for the SBO with the N model. Figure 10 demonstrates the nearly identical phosphate concentrations predicted by the ANN for the three parameter vectors  $\mathbf{u}_0, \bar{\mathbf{u}}, \tilde{\mathbf{u}} \in \mathbb{R}^{n_u}$  defined in Table 2. Consequently, the steady annual cycles calculated as spin-up over one model year using the prediction as an initial concentration differed only marginally from each other due to the different model parameters. Instead of the high-fidelity solution of the corresponding parameter vector, the surrogate, therefore, in each case, approximated the high-fidelity solution for parameter vector  $\mathbf{u}_0$  with which surrogate  $\mathbf{s}_0$  was constructed. We observed a similar behavior using random parameter vectors in a small area around the reference parameters used to construct the surrogate.

The SBO did not identify any model parameters. After three surrogate optimizations,

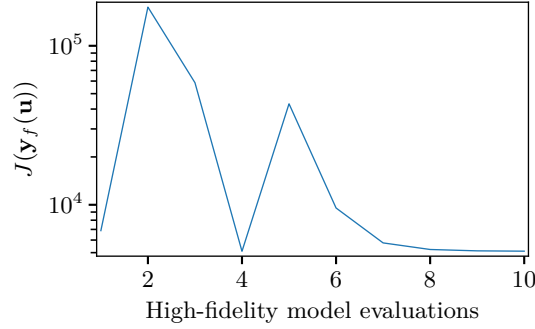


Figure 11: Convergence of the cost function value  $J(\mathbf{y}_f)$  for the exemplary SBO run with the N model using the prediction of the ANN as low-fidelity model ( $\mathbf{y}_c^{\text{ANN}}$ ). The iterations 0 and 1 (with parameter vectors  $\mathbf{u}_0$  and  $\mathbf{u}_1$ ) of the SBO run correspond to 1 and 4 evaluations of the high-fidelity model, respectively.

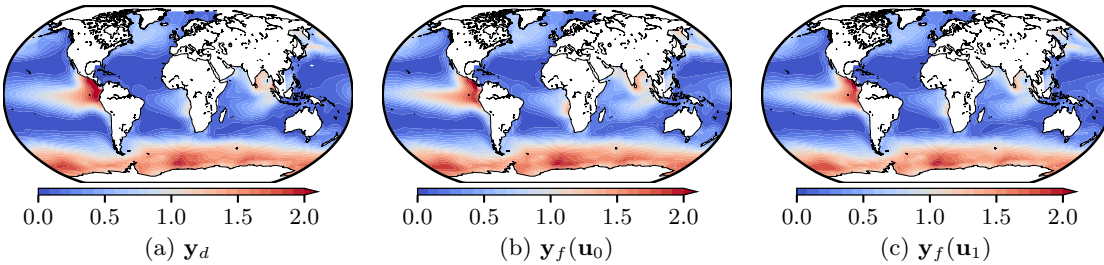


Figure 12: High-fidelity model output  $\mathbf{y}_f$  obtained by the exemplary SBO run with the N model using the prediction of the ANN as low-fidelity model ( $\mathbf{y}_c^{\text{ANN}}$ ) at the beginning and after one iteration (i.e., evaluated with the parameter vectors  $\mathbf{u}_0$  and  $\mathbf{u}_1$ ) as well as the target data  $\mathbf{y}_d$ . Shown are the phosphate concentrations on the surface layer (0 m to 50 m) at the first time step of the model year (in January).

the SBO calculated with surrogate  $\mathbf{s}_0$  just one parameter vector  $\mathbf{u}_1 \in \mathbb{R}^{n_u}$  for which the corresponding reference cost function value was smaller than for the initial parameter vector  $\mathbf{u}_0$  (Figure 11). The subsequent surrogate optimizations with surrogate  $\mathbf{s}_1$  did not yield a parameter vector whose high-fidelity model solution approximated the target data better. Although the main pattern of the target phosphate concentration for the high-fidelity solution corresponding to the parameter vector  $\mathbf{u}_0$  as well as  $\mathbf{u}_1$  were evident as seen in Figure 12, there were many differences, such as in the Pacific, and, consequently, parameter vector  $\mathbf{u}_1$  did not provide a satisfactory identification of the optimal parameter vector  $\mathbf{u}_d$ . After only one iteration and ten high-fidelity model evaluations, the SBO terminated because the trust-region radius was decreased in every step using  $m_{\text{decr}} = 4$  and, hence, fell below the threshold  $\delta^{\text{min}}$  after ten steps.

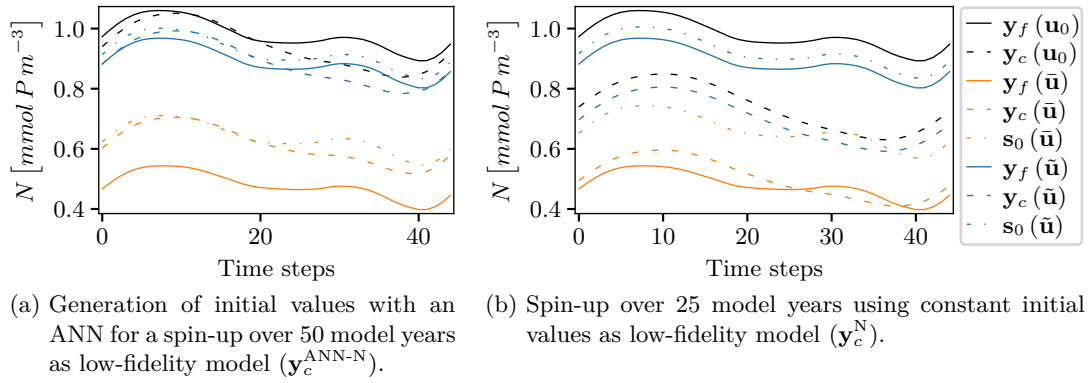


Figure 13: Annual cycle of phosphate for the high- ( $\mathbf{y}_f$ ), low-fidelity model ( $\mathbf{y}_c$ ) and surrogate ( $\mathbf{s}_0$ ) on the surface layer (0 m to 50 m) for the location 120.9375° W, 30.9375° N. Shown are the annual cycles for three parameter values  $\mathbf{u}_0$  (as “reference point”),  $\bar{\mathbf{u}}$  (a neighbouring point) and  $\tilde{\mathbf{u}}$  (a point in a closer vicinity) defined in Table 2. The surrogate is built using parameter vector  $\mathbf{u}_0$ , the reason why the solution of the surrogate is omitted at the reference point.

## 5.5 ANN as initial value generator for the low-fidelity model

Using the prediction of the ANN as initial concentration for a spin-up over 50 model years as low-fidelity model (see Section 4.2.3) was reasonable to construct a reliable surrogate in conjunction with the multiplicative response correction for the SBO using the N model. The annual cycles of phosphate in Figure 13 indicate an almost equivalent approximation of the high-fidelity model concentration by the surrogates using, on the one hand, the low-fidelity model with initial concentration predicted by the ANN and, on the other hand, the low-fidelity model with constant initial concentrations. Although the concentrations differed for both low-fidelity models, the multiplicative correction technique improved the accuracy of the low-fidelity models and resulted in nearly the same approximation.

The parameter identification using the SBO identified four out of five model parameters of the N model. Figure 14 shows the convergence of the tracer concentrations to the target data  $\mathbf{y}_d$  using different step sizes during the optimization. Except for parameter  $K_I$ , the single parameters converged to the parameter values of the optimal parameter vector  $\mathbf{u}_d$  (Figure 15). As a result of a step size less than the threshold  $\gamma$ , the SBO terminated after 20 iterations. For this optimization run, we applied parameters  $m_{\text{incr}} = 2$  and  $m_{\text{decr}} = 2$  for the update of the trust-region radius. Figures 16 and 17 illustrate the continuous improvement of the agreement of the high-fidelity solution and the target data during the optimization.

The computational effort of the parameter identification using the SBO was low. To obtain parameter vector  $\mathbf{u}_{20}$ , the SBO required 35 high-fidelity model evaluations and about 8000 evaluations of the surrogate. In the exemplary SBO run, the surrogate optimization needed up to 50 iterations. Indeed, the number of surrogate evaluations

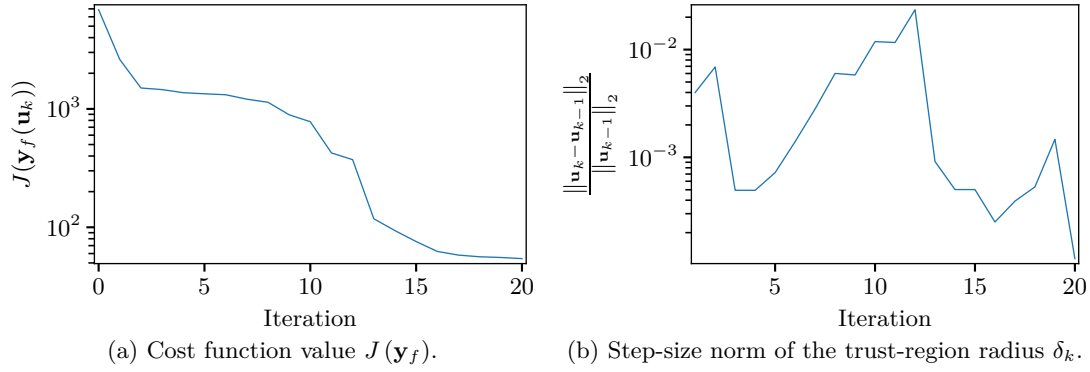


Figure 14: Convergence of the cost function value and the step-size norm of the trust-region radius for the exemplary SBO run with the prediction of the ANN as initial concentration for the spin-up as low-fidelity model ( $\mathbf{y}_c^{\text{ANN-N}}$ ).

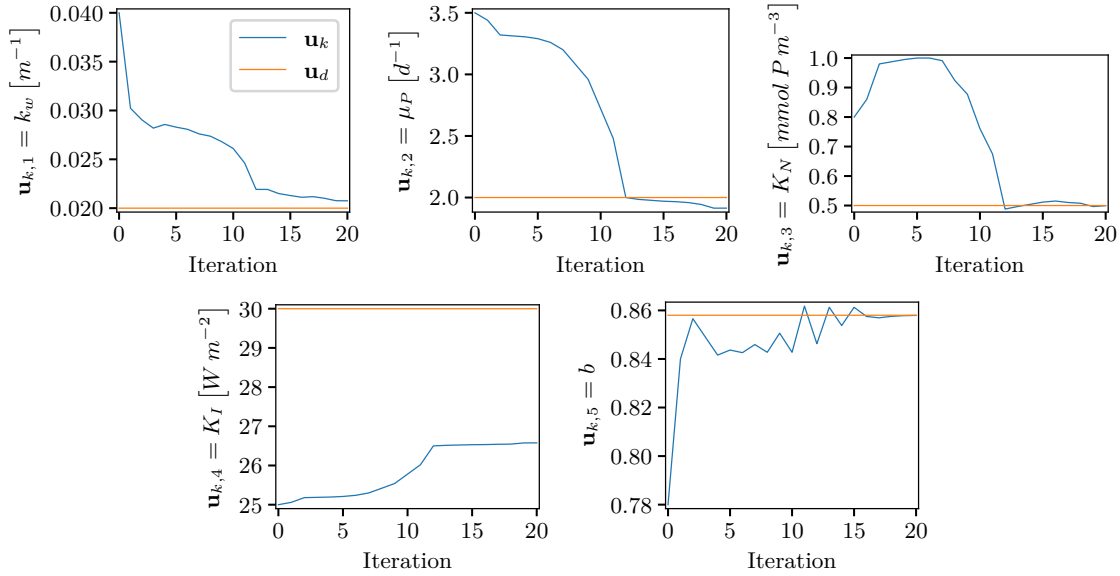


Figure 15: Convergence of the single parameter values  $\mathbf{u}_{k,i}$  for each iteration of the exemplary SBO run with the prediction of the ANN as initial concentration for the spin-up as low-fidelity model ( $\mathbf{y}_c^{\text{ANN-N}}$ ).

could be reduced if we restricted the iterations for each surrogate optimization to ten. Apart from reducing computational costs, the limitation of the iterations did not lead to an adequate identification of the model parameters because the cost function reached a value of 1300 only.

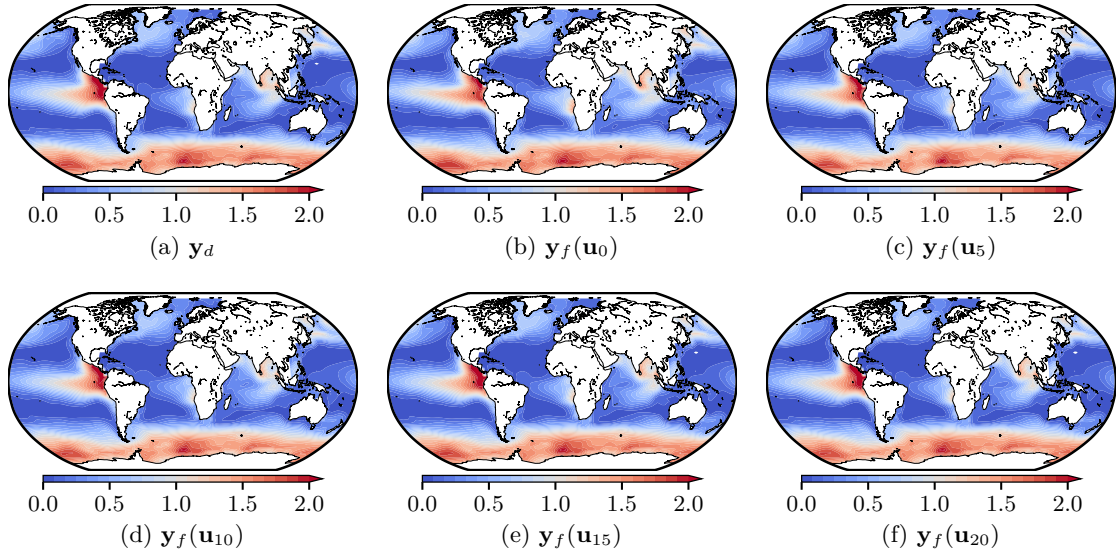


Figure 16: High-fidelity model output  $\mathbf{y}_f$  obtained by the exemplary SBO run with the prediction of the ANN as initial concentration for the spin-up as low-fidelity model ( $\mathbf{y}_c^{\text{ANN-N}}$ ) at the beginning and after 5, 10, 15 and 20 iterations (i.e., evaluated with the parameter vectors  $\mathbf{u}_0$ ,  $\mathbf{u}_5$ ,  $\mathbf{u}_{10}$ ,  $\mathbf{u}_{15}$  and  $\mathbf{u}_{20}$ ) as well as the target data  $\mathbf{y}_d$ . Shown are the phosphate concentrations on the surface layer (0 m to 50 m) at the first time step of the model year (in January).

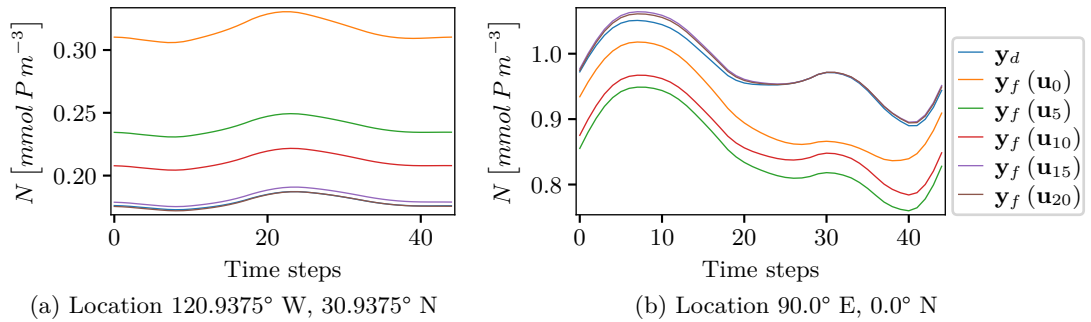


Figure 17: Annual cycles of phosphate of the high-fidelity model output  $\mathbf{y}_f$  obtained by the exemplary SBO run with the prediction of the ANN as initial concentration for the spin-up as low-fidelity model ( $\mathbf{y}_c^{\text{ANN-N}}$ ) at the beginning and after 5, 10, 15 and 20 iterations (i.e., evaluated with the parameter vectors  $\mathbf{u}_0$ ,  $\mathbf{u}_5$ ,  $\mathbf{u}_{10}$ ,  $\mathbf{u}_{15}$  and  $\mathbf{u}_{20}$ ) as well as the target data  $\mathbf{y}_d$  on the surface layer (0 m to 50 m) for two distinct locations.

## 6 Conclusions

The SBO is based on a low-fidelity model that, on the one hand, can be evaluated computationally inexpensive and, on the other hand, is an appropriate approximation of the high-fidelity model. A suitable correction technique improves additionally the accuracy of the low-fidelity model building the surrogate. We have compared three different low-fidelity models in conjunction with the multiplicative response correction already employed by Prieß, Piwonski, et al. (2013). In addition to the truncated spin-up (Prieß, Piwonski, et al. 2013), we applied a neural network only and in combination with the truncated spin-up as low-fidelity model.

Using the SBO, the parameter optimization yielded similar results for the low-fidelity models including and excluding the application of the neural network except for the direct use of the prediction. With the exception of model parameter  $K_I$  modeling the light intensity compensation, the SBO identified all model parameters for both biogeochemical models and confirmed the results of Prieß, Piwonski, et al. (2013) for the N-DOP model. However, the parameter identifications were not optimal. A reason for the mismatch, on the one hand, was possibly the low accuracy of the underlying low-fidelity model as well as a weak sensitivity with regard to the model parameters as already observed by Rückelt et al. (2010) for a different biogeochemical model. For instance, the construction of the surrogate considering information about the high-fidelity model could increase the accuracy. On the other hand, the trust region radius limited the convergence of parameter  $K_I$  because the admissible parameter range of this parameter was much larger than for the other parameters and, thus, larger adjustments were necessary.

The use of neural networks to construct the surrogate reduced significantly the computational costs of a parameter optimization. A reduction of these costs is desirable because a parameter identification in climate models is very expensive (Kwon and Primeau 2006; Kwon and Primeau 2008; Mattern, K. Fennel, and Dowd 2012). Indeed, the SBO, however, reduces the computational costs compared to standard optimization routines but the reduction of costs for the low-fidelity model decreases these further. If a neural network is available, the computational costs of the prediction are negligible. Therefore, the costs only originated from the subsequent truncated spin-up, if this was used. However, the prediction of the ANN alone was not suitable as low-fidelity model because only minimal concentration changes arose from the prediction using various parameter vectors in a small environment. A neural network trained with parameter vectors in such a small environment, nevertheless, had the ability to predict the concentrations reasonably for a random parameter vector of this environment whereas the prediction was often insufficient for parameter vectors outside this environment. The training of a neural network, furthermore, is computationally costly and depends on the availability of a sufficient amount of training data. Future work should, therefore, include the training of an ANN that better predicts the concentrations locally and, thus, serves as low-fidelity model for the construction of a reliable surrogate with the multiplicative correction. For this purpose, reinforcement learning (Sutton and Barto 2018; Mnih et al. 2015) could help to continuously improve the neural network during an optimization run. Moreover, further future work should include the application of the SBO for parameter identification using

a normalization of the admissible parameter range for each component of the parameter vector as well as using real measurement data that, for example, is necessary for model assessment (see e.g., Kriest, Khatiwala, and Oschlies 2010) and model calibration (see e.g., Kriest, Sauerland, et al. 2017; Kriest 2017).

In summary, the main points of this paper are the following:

- Using the truncated spin-up as a low-fidelity model, the SBO was a computationally efficient method for the parameter identification of marine ecosystem models.
- The prediction of the presented ANN as low-fidelity model was unsuitable for an SBO.
- Using the prediction of the ANN as an initial concentration for a truncated spin-up, the low-fidelity model represented an acceptable alternative to the truncated spin-up with slightly higher computational costs.

## Code and data availability

The code used to generate the data in this publication is available at <https://github.com/slavig/bgc-ann> and <https://metos3d.github.io/>. All used and generated data are available at <https://doi.org/10.5281/zenodo.5643667> (Pfeil and Slawig 2021b).

## References

- Bacastow, Robert B. and Ernst Maier-Reimer (Apr. 1990). “Ocean-circulation model of the carbon cycle”. In: *Climate Dynamics* 4.2, pp. 95–125. DOI: 10.1007/BF00208905.
- (1991). “Dissolved organic carbon in modeling oceanic new production”. In: *Global Biogeochemical Cycles* 5.1, pp. 71–85. DOI: 10.1029/91GB00015.
- Bandler, John W. et al. (2004). “Space mapping: the state of the art”. In: *IEEE Transactions on Microwave Theory and Techniques* 52.1, pp. 337–361. DOI: 10.1109/TMTT.2003.820904.
- Banks, Harvey Thomas and Karl Kunisch (1989). *Estimation Techniques for Distributed Parameter Systems*. Systems and Control: Foundations and Applications. Basel: Birkhäuser. DOI: 10.1007/978-1-4612-3700-6.
- Bernsen, Erik, Henk A. Dijkstra, and Fred W. Wubs (2008). “A method to reduce the spin-up time of ocean models”. In: *Ocean Modelling* 20.4, pp. 380–392. DOI: 10.1016/j.ocemod.2007.10.008.
- Bottou, Léon and Olivier Bousquet (2008). “The Tradeoffs of Large Scale Learning”. In: *Advances in Neural Information Processing Systems*. Ed. by John C. Platt et al. Vol. 20. NIPS’07. Curran Associates Inc., pp. 161–168.
- Bryan, Kirk (1984). “Accelerating the Convergence to Equilibrium of Ocean-Climate Models”. In: *Journal of Physical Oceanography* 14.4, pp. 666–673. DOI: 10.1175/1520-0485(1984)014<0666:ATCTEO>2.0.CO;2.

- Byrd, Richard H. et al. (1995). “A Limited Memory Algorithm for Bound Constrained Optimization”. In: *SIAM Journal on Scientific Computing* 16.5, pp. 1190–1208. DOI: 10.1137/0916069.
- Clevert, Djork-Arné, Thomas Unterthiner, and Sepp Hochreiter (2015). *Fast and Accurate Deep Network Learning by Exponential Linear Units (ELUs)*. Preprint on arXiv. arXiv: 1511.07289 [cs.LG].
- Conn, Andrew R., Nicholas I. M. Gould, and Philippe L. Toint (2000). *Trust Region Methods*. MOS-SIAM Series on Optimization. Society for Industrial and Applied Mathematics. DOI: 10.1137/1.9780898719857.
- Danabasoglu, Gokhan, James C. McWilliams, and William G. Large (1996). “Approach to Equilibrium in Accelerated Global Oceanic Models”. In: *Journal of Climate* 9.5, pp. 1092–1110. DOI: 10.1175/1520-0442(1996)009<1092:ATEIAG>2.0.CO;2.
- Fasham, Michael J. R., ed. (2003). *Ocean Biogeochemistry. The Role of the Ocean Carbon Cycle in Global Change*. Global Change – The IGBP Series. Berlin et al.: Springer. DOI: 10.1007/978-3-642-55844-3.
- Fennel, Katja et al. (2001). “Testing a marine ecosystem model: sensitivity analysis and parameter optimization”. In: *Journal of Marine Systems* 28.1, pp. 45–63. DOI: 10.1016/S0924-7963(00)00083-X.
- Fennel, Wolfgang and Thomas Neumann (2004). *Introduction to the Modelling of Marine Ecosystems*. Vol. 72. Elsevier Oceanography Series. Elsevier.
- Forrester, Alexander I.J. and Andy J. Keane (2009). “Recent advances in surrogate-based optimization”. In: *Progress in Aerospace Sciences* 45.1, pp. 50–79. DOI: 10.1016/j.paerosci.2008.11.001.
- Goodfellow, Ian, Yoshua Bengio, and Aaron Courville (2016). *Deep Learning*. Adaptive computation and machine learning. MIT Press.
- Hastie, Trevor, Robert Tibshirani, and Jerome Friedman (2009). *The elements of statistical learning. Data Mining, Inference, and Prediction*. 2nd ed. Springer Series in Statistics. New York, NY: Springer, p. 745. DOI: 10.1007/978-0-387-84858-7.
- Khatiwala, Samar (2007). “A computational framework for simulation of biogeochemical tracers in the ocean”. In: *Global Biogeochemical Cycles* 21.3. DOI: 10.1029/2007GB002923.
- Khatiwala, Samar, Martin Visbeck, and Mark A. Cane (2005). “Accelerated simulation of passive tracers in ocean circulation models”. In: *Ocean Modelling* 9.1, pp. 51–69. DOI: 10.1016/j.ocemod.2004.04.002.
- Klambauer, Günter et al. (2017). “Self-Normalizing Neural Networks”. In: *Advances in Neural Information Processing Systems*. Ed. by Isabelle Guyon et al. Vol. 30. Curran Associates, Inc., pp. 971–980.
- Koziel, Slawomir, John W. Bandler, and Qingsha S. Cheng (2010). “Robust Trust-Region Space-Mapping Algorithms for Microwave Design Optimization”. In: *IEEE Transactions on Microwave Theory and Techniques* 58.8, pp. 2166–2174. DOI: 10.1109/TMTT.2010.2052666.
- Kriest, Iris (2017). “Calibration of a simple and a complex model of global marine biogeochemistry”. In: *Biogeosciences* 14.21, pp. 4965–4984. DOI: 10.5194/bg-14-4965-2017.

- Kriest, Iris, Samar Khatiwala, and Andreas Oschlies (2010). “Towards an assessment of simple global marine biogeochemical models of different complexity”. In: *Progress In Oceanography* 86.3-4, pp. 337–360. DOI: 10.1016/j.pocean.2010.05.002.
- Kriest, Iris, Volkmar Sauerland, et al. (2017). “Calibrating a global three-dimensional biogeochemical ocean model (MOPS-1.0)”. In: *Geoscientific Model Development* 10.1, pp. 127–154. DOI: 10.5194/gmd-10-127-2017.
- Kwon, Eun Young and François Primeau (2006). “Optimization and sensitivity study of a biogeochemistry ocean model using an implicit solver and in situ phosphate data”. In: *Global Biogeochemical Cycles* 20.4. DOI: 10.1029/2005GB002631.
- (2008). “Optimization and sensitivity of a global biogeochemistry ocean model using combined in situ DIC, alkalinity, and phosphate data”. In: *Journal of Geophysical Research: Oceans* 113.C8. DOI: 10.1029/2007JC004520.
- LeCun, Yann, Yoshua Bengio, and Geoffrey Hinton (2015). “Deep learning”. In: *Nature* 521, pp. 436–444. DOI: 10.1038/nature14539.
- Lee, Abraham (2014). *pyDOE: Design of Experiments for Python*. available at: <https://pythonhosted.org/pyDOE/index.html> (last access: November 30, 2021).
- Leifsson, Leifur and Slawomir Koziel (2010). “Multi-fidelity design optimization of transonic airfoils using shape-preserving response prediction”. In: *Procedia Computer Science* 1.1. ICCS 2010, pp. 1311–1320. DOI: 10.1016/j.procs.2010.04.146.
- Lotka, Alfred James (1910). “Contribution to the Theory of Periodic Reactions”. In: *The Journal of Physical Chemistry* 14.3, pp. 271–274. DOI: 10.1021/j150111a004.
- Marshall, John et al. (1997). “A finite-volume, incompressible Navier Stokes model for studies of the ocean on parallel computers”. In: *Journal of Geophysical Research: Oceans* 102.C3, pp. 5753–5766. DOI: 10.1029/96JC02775.
- Martin, John H. et al. (1987). “VERTEX: carbon cycling in the northeast Pacific”. In: *Deep Sea Research Part A. Oceanographic Research Papers* 34.2, pp. 267–285. DOI: 10.1016/0198-0149(87)90086-0.
- Mattern, Jann Paul, Katja Fennel, and Michael Dowd (2012). “Estimating time-dependent parameters for a biological ocean model using an emulator approach”. In: *Journal of Marine Systems* 96-97, pp. 32–47. DOI: 10.1016/j.jmarsys.2012.01.015.
- McGuffie, Kendal and Ann Henderson-Sellers (2014). *The Climate Modelling Primer*. 4th ed. Chichester, West Sussex, United Kingdom: John Wiley & Sons.
- McKay, Michael D., Richard J. Beckman, and William Jay Conover (1979). “A Comparison of Three Methods for Selecting Values of Input Variables in the Analysis of Output from a Computer Code”. In: *Technometrics* 21.2, pp. 239–245. DOI: 10.2307/1268522.
- Mnih, Volodymyr et al. (2015). “Human-level control through deep reinforcement learning”. In: *Nature* 518.7540, pp. 529–533. DOI: 10.1038/nature14236.
- Oschlies, Andreas (2006). “On the use of data assimilation in biogeochemical modelling”. In: *Ocean Weather Forecasting*. Ed. by E. P. Chassignet and J. Verron. Dordrecht: Springer, pp. 525–547. DOI: 10.1007/1-4020-4028-8\_24.
- Paltridge, Garth William and C. M. R. Platt (1976). *Radiative Processes in Meteorology and Climatology*. New York: Elsevier. DOI: 10.1002/qj.49710343713.

- Parekh, P., Michael J. Follows, and Edward A. Boyle (2005). “Decoupling of iron and phosphate in the global ocean”. In: *Global Biogeochemical Cycles* 19.2. DOI: 10.1029/2004GB002280.
- Pfeil, Markus and Thomas Slawig (2021a). “Approximation of a marine ecosystem model by artificial neural networks”. In: *Electronic Transactions on Numerical Analysis*. accepted.
- (2021b). *Surrogate-based optimization using an artificial neural network for a parameter identification in a 3D marine ecosystem model*. Version 1.0. Zenodo. DOI: 10.5281/zenodo.5643667.
- Piwonski, Jaroslaw and Thomas Slawig (2016). “Metos3D: the Marine Ecosystem Toolkit for Optimization and Simulation in 3-D – Part 1: Simulation Package v0.3.2”. In: *Geoscientific Model Development* 9.10, pp. 3729–3750. DOI: 10.5194/gmd-9-3729-2016.
- Prieß, Malte, Slawomir Koziel, and Thomas Slawig (2011). “Surrogate-based optimization of climate model parameters using response correction”. In: *Journal of Computational Science* 2.4, pp. 335–344. DOI: 10.1016/j.jocs.2011.08.004.
- (2013). “Marine Ecosystem Model Calibration through Enhanced Surrogate-Based Optimization”. In: *Simulation and Modeling Methodologies, Technologies and Applications*. Ed. by Nuno Pina, Janusz Kacprzyk, and Joaquim Filipe. Vol. 197. Advances in Intelligent Systems and Computing. Berlin, Heidelberg: Springer, pp. 193–208. DOI: 10.1007/978-3-642-34336-0\_13.
- Prieß, Malte, Jaroslaw Piwonski, et al. (2013). “Accelerated parameter identification in a 3D marine biogeochemical model using surrogate-based optimization”. In: *Ocean Modelling* 68, pp. 22–36. DOI: 10.1016/j.ocemod.2013.04.003.
- Queipo, Nestor V. et al. (2005). “Surrogate-based analysis and optimization”. In: *Progress in Aerospace Sciences* 41.1, pp. 1–28. DOI: 10.1016/j.paerosci.2005.02.001.
- Rückelt, Johannes et al. (2010). “Parameter optimization and uncertainty analysis in a model of oceanic CO<sub>2</sub> uptake using a hybrid algorithm and algorithmic differentiation”. In: *Nonlinear Analysis: Real World Applications* 11.5, pp. 3993–4009. DOI: 10.1016/j.nonrwa.2010.03.006.
- Rumelhart, David E., Geoffrey E. Hinton, and Ronald J. Williams (1986). “Learning representations by back-propagating errors”. In: *Nature* 323.6088, pp. 533–536. DOI: 10.1038/323533a0.
- Sarmiento, Jorge Louis and Nicolas Gruber (2006). *Ocean biogeochemical dynamics*. Princeton et al.: Princeton University Press, p. 528.
- Siberlin, Charlotte and Carl Wunsch (2011). “Oceanic tracer and proxy time scales revisited”. In: *Climate of the Past* 7.1, pp. 27–39. DOI: 10.5194/cp-7-27-2011.
- Simpson, T. W. et al. (2001). “Metamodels for Computer-based Engineering Design: Survey and recommendations”. In: *Engineering with Computers* 17.2, pp. 129–150. DOI: 10.1007/PL00007198.
- Smola, Alex J. and Bernhard Schölkopf (2004). “A tutorial on support vector regression”. In: *Statistics and Computing* 14.3, pp. 199–222. DOI: 10.1023/B:STCO.0000035301.49549.88.

- Søndergaard, Jacob (2003). “Optimization using surrogate models - by the space mapping technique”. Supervisor: Kaj Madsen. Richard Petersens Plads, Building 321, DK-2800 Kgs. Lyngby: Informatics and Mathematical Modelling, Technical University of Denmark, DTU, p. 203. URL: <http://www2.compute.dtu.dk/pubdb/pubs/2450-full.html>.
- Sutton, Richard S. and Andrew G. Barto (2018). *Reinforcement Learning: An Introduction*. Second. Adaptive Computation and Machine Learning series. Cambridge, MA, USA: MIT Press.
- Virtanen, Pauli et al. (2020). “SciPy 1.0: Fundamental Algorithms for Scientific Computing in Python”. In: *Nature Methods* 17, pp. 261–272. DOI: 10.1038/s41592-019-0686-2.
- Volterra, Vito (1931). “Variations and fluctuations of the number of individuals in animal species living together”. In: *Animal Ecology*. Ed. by R. N. Chapman. New York: McGraw-Hill, pp. 409–448.
- Wunsch, Carl and Patrick Heimbach (2008). “How long to oceanic tracer and proxy equilibrium?” In: *Quaternary Science Reviews* 27.7, pp. 637–651. DOI: 10.1016/j.quascirev.2008.01.006.
- Zhu, Ciyu et al. (1997). “Algorithm 778: L-BFGS-B: Fortran Subroutines for Large-Scale Bound-Constrained Optimization”. In: *ACM Trans. Math. Softw.* 23.4, pp. 550–560. DOI: 10.1145/279232.279236.